Redox Biology 61 (2023) 102648

Contents lists available at ScienceDirect

Redox Biology

journal homepage: www.elsevier.com/locate/redox

Meta-data analysis of kidney stone disease highlights ATP1A1 involvement in renal crystal formation

Yang Li [a,b,1], Xiuli Lu [a,1], Zhihao Yu [b], Haozhen Wang [a], Bing Gao [b,*]

[a] Department of Biochemistry and Molecular Biology, Life Science School, Liaoning University, Shenyang, 110036, China
[b] Department of Cell biology and Genetics, Shenyang Medical College, Shenyang 110034, China

ARTICLE INFO

Keywords:
Nephrolithiasis
Gene expression
Oxidative stress
DNA methylation

ABSTRACT

Nephrolithiasis is a complicated disease affected by various environmental and genetic factors. Crystal-cell adhesion is a critical initiation process during kidney stone formation. However, genes regulated by environmental and genetic factors in this process remain unclear. In the present study, we integrated the gene expression profile data and the whole-exome sequencing data of patients with calcium stones, and found that *ATP1A1* might be a key susceptibility gene involved in calcium stone formation. The study showed that the T-allele of rs11540947 in the 5′-untranslated region of *ATP1A1* was associated with a higher risk of nephrolithiasis and lower activity of a promoter of *ATP1A1*. Calcium oxalate crystal deposition decreased ATP1A1 expression *in vitro* and *in vivo* and was accompanied by the activation of the ATP1A1/Src/ROS/p38/JNK/NF-κB signaling pathway. However, the overexpression of ATP1A1 or treatment with pNaKtide, a specific inhibitor of the ATP1A1/Src complex, inhibited the ATP1A1/Src signal system and alleviated oxidative stress, inflammatory responses, apoptosis, crystal-cell adhesion, and stone formation. Moreover, the DNA methyltransferase inhibitor 5-aza-2′-deoxycytidine reversed ATP1A1 down-regulation induced by crystal deposition. In conclusion, this is the first study to show that *ATP1A1*, a gene modulated by environmental factors and genetic variations, plays an important role in renal crystal formation, suggesting that *ATP1A1* may be a potential therapeutic target for treating calcium stones.

1. Introduction

Nephrolithiasis (or kidney stone) is a common health issue affecting people across the world and is attributable to environmental and genetic factors, with an increasing incidence and recurrence rate. The majority of nephrolithiasis is composed of calcium oxalate (CaOx) stone(s), often admixed with some calcium phosphate (CaP) as the initial nidus of the stone [1]. Although several different hypotheses have been proposed regarding the theory of stone formation, crystal-cell adhesion is recognized as the key process for crystal retention and stone formation [2,3]. Previous evidence suggests that damaged renal tubular epithelial cells increase the affinity for crystal attachment and that crystal deposition, in turn, induces cell injury and inflammatory responses through the production of excessive reactive oxygen species (ROS) [4–7]. However, crystal-cell adhesion is a complex process, and all the key genes involved in this process are not yet known.

Na/K-ATPase (NKA) is a transmembrane ion pump that is highly expressed in the kidney. It pumps three Na^+ out of the cell in exchange for two K^+ into the cell by hydrolyzing one ATP molecule, thereby creating an electrochemical gradient that drives the activity of Na^+-dependent transporters in the proximal tubules, which is deemed essential for several cellular functions, such as nutrient uptake and urine excretion [8,9]. In addition to an ion pump, NKA also serves as a classical signal transducer owing to its α1 subunit, encoded by *ATP1A1*, which exerts a tissue-protecting effect by promoting growth and inhibiting apoptosis [10]. In the resting condition, the α1 subunit is coupled

Abbreviations: CaOx, Calcium oxalate; CaP, Calcium phosphate; ROS, Reactive oxygen species; NKA, Na/K-ATPase; CTSs, Cardiotonic steroids; WGCNA, Weighted gene co-expression network analysis; UTR, Untranslated region; 5Aza-2dc, 5-aza-2'-deoxycytidine; DCFHDA, 2′, 7′-dichloroflfluorescin diacetate; COM, Calcium oxalate monohydrate; HYP, Hydroxyproline; CASR, Calcium-sensing receptor; VDR, Vitamin D receptor; OPN, Osteopontin; GWAS, Genome-wide association studies; WES, Whole-exome sequencing; HRM, High-resolution melting.

* Corresponding author. Department of Cell biology and Genetics, Shenyang Medical College, Huanghe North Street No.146, Shenyang, 110034, China.
E-mail address: gaobingdr@hotmail.com (B. Gao).

[1] Yang Li and Xiuli Lu contributed equally to this work.

https://doi.org/10.1016/j.redox.2023.102648
Received 1 December 2022; Received in revised form 11 February 2023; Accepted 25 February 2023
Available online 27 February 2023

with sarcoma-related kinase Src to form a receptor complex so as to retain Src in an inactivated state [11]. Once ligands, such as cardiotonic steroids (CTSs) and hydrogen peroxide, bind to ATP1A1 to change its conformation or when *ATP1A1* is knocked down, Src gets phosphorylated and activates the downstream signaling cascades, which, in turn, lead to the generation of ROS [11–14]. ROS can activate the MAPK cascade and NF-κB inflammatory response as well as initiate the ATP1A1/Src signaling pathway as a ligand of ATP1A1 so as to form an NKA/ROS amplification loop to induce oxidative stress [15,16].

NKA activity and signaling are associated with many diseases. Xiao et al. found that impaired NKA signaling contributed to hyperuricemia-induced renal tubular injury by regulating Src, NLRP3, and IL-1β [17]. Bartlett et al. demonstrated that uremic toxins accumulation resulting from experimental chronic kidney diseases activated the NKA/ROS amplification loop, causing phenotypic alterations in adipocytes [18]. *ATP1A1* gene polymorphism is also involved in some disease progressions. A synonymous G94A SNP at nucleotide 27 in the exon 2 of *ATP1A1* (rs1060366) was associated with type 2 diabetes mellitus and diabetic neuropathy among Egyptian patients [19]. The whole exome sequencing (WES) of aldosterone-producing adenomas showed two missense mutations in *ATP1A1* (c.311T > G and c.995T > G, resulting in p.Leu104Arg and p.Val332Gly, respectively) that could impair the NKA ion pump activity, decrease affinity for K^+, and increase intracellular Ca^{2+} concentration, thus probably promoting calcium-dependent signal transduction and aldosterone output [20]. The *ATP1A1 de novo* mutations c.2797G > A[p.Asp933Asn] and c.2590G > A[p.Gly864Arg] (NM_000701) were correlated to developmental delays [21]. However, the role of ATP1A1 in kidney stone formation remains unclear.

Recent omics studies, including genome-wide association studies (GWAS), WES, gene expression profiles, the proteomics research, have established effective methods for searching nephrolithiasis-susceptibility genes and the related pathogenesis [22–25]. However, a single omics study cannot adequately explain the entire disease process. Therefore, multiple omics analyses should be undertaken to provide a helpful approach investigating the precise disease pathophysiology [26]. In the present study, to explore the key susceptibility genes involved in nephrolithiasis from the genetic level and the transcriptional level affected by environmental factors, we integrated the gene expression profiles data of Randall's plaque (RP) tissues from calcium stone formers with the WES data of CaOx patients and identified *ATP1A1* [23]. We also investigated the association of *ATP1A1* genetic variation with the risk of calcium stones and further explored the roles of ATP1A1/Src/ROS signaling in kidney stone formation both *in vitro* and *in vivo*. This study's finding revealed the mechanism through which *ATP1A1* genetic variation and its reduced expression are involved in the renal crystal formation, which may provide a potential therapeutic target for CaOx stones.

2. Materials and methods

2.1. Gene expression profiles data processing

The gene expression profiles of GSE73680 were downloaded from the Gene Expression Omnibus (GEO) database. GSE73680 consisted of 62 samples from the renal papillary RP and normal tissues of 29 patients with calcium stones, including 23 CaOx stone formers and 6 CaP stone formers, and normal papillary tissues of 7 controls without any kidney stones. The RP tissues from these calcium stone formers were designated as the P group (n = 29), normal papillary tissues from these calcium stone formers were designated as the N group (n = 27), and normal papillary tissues from the controls were designated as the C group (n = 6) [23]. We analyzed gene expression in the N and P groups (n = 56), which was crucial for analyzing kidney stone formation. First, the quality of all samples was evaluated using the "limma" package of the R language, and four abnormal samples were excluded by constructing a boxplot. Then, the remaining sample data were analyzed by weighted gene co-expression network analysis (WGCNA) using the WGCNA R package, and the correlation between gene modules and the disease phenotype was established. Finally, all genes from the nephrolithiasis-related module were extracted for gene ontology (GO) analysis and KEGG enrichment analysis with the "DAVID Bioinformatics Resources" (https://david-d.ncifcrf.gov/tools.jsp). The GO terms included biological processes (BP), cellular components (CC), and molecular functions (MF).

2.2. Whole exome sequencing

Genomic DNA samples from 28 Chinese Han patients with CaOx stones were fragmented and captured by using the SureSelect Human All Exon v6 kit (Agilent Technologies). These patients included 22 men and 6 women, with a mean ± SD age of 53.32 ± 10.50 years. The enriched DNA fragments were paired-end sequenced by using the Illumina HiSeq X Ten sequencing platform. The clean reads with high quality were then mapped to the human reference genome (hg 19) by using the Burrows-Wheeler Aligner (BWA). SNP detection and annotation were performed with the GATK and ANNOVAR software, respectively. The variants were then filtered against the 1000 Genomes sequencing project. The WES was carried out by Biomarker Technologies CO. Ltd. (Beijing, China). SNPs with $p < 0.005$ were considered as the candidate variants. The study was approved by the Shenyang Medical College Institutional Review Boards and the informed consents were obtained from all participants.

2.3. Integrating analysis of the gene expression profile and the WES data

The missense SNPs, coding-synonymous SNPs, as well as SNPs in 5′-untranslated region (UTR) and 3′UTR, with a p value less than 0.005, were selected from the WES data and mapped to genes, which were integrated with genes in the salmon module of WGCNA analysis for Venn diagram analysis with the online VENNY 2.1 (https://bioinfogp.cnb.csic.es/tools/venny/index.html).

2.4. Study participants for genotyping with high-resolution melting (HRM) analysis

This study assessed 214 unrelated patients with calcium stone (143 men, 71 women; mean ± SD age: 54.28 ± 13.10 years). The stone composition was identified by Fourier-transformed infrared spectroscopy. The control group included 232 unrelated normal participants (142 men, 90 women; mean ± SD age: 65.17 ± 13.08 years), who had no history of nephrolithiasis or family nephrolithiasis. All controls were confirmed through a general physical examination. Cases of non-calcium stones, hyperparathyroidism, and urinary tract infection were strictly eliminated based on the results of the stone composition analysis, serial blood, and urine biochemistry assays. All participants in the present study are Chinese Han people. The study was approved by the Shenyang Medical College Institutional Review Boards and informed consent was obtained from all participants. Genomic DNA was extracted from peripheral blood by using the RelaxGene Blood DNA System (Tiangen, China).

2.5. HRM analysis

Genotyping for rs11540947 (C > T) in *ATP1A1* was performed in a 96-well plate by using the HRM analysis kit (Tiangen, China) according to the manufacturer's recommendation. The human *ATP1A1* (*hATP1A1*) forward primer was 5′- GCCCTAGCTCCCTCCACTTG-3′, and the *hATP1A1* reverse primer was 5′-GGGTCCTGTCGCTGGAGAAT-3'. Three samples with CC, CT, and TT identified with Sanger sequencing were selected as the positive controls. For each experiment, the normalization settings and reference genotype were kept the same. Each sample was performed at least three times independently.

2.6. Site-directed mutagenesis of rs11540947 (C > T)

SNPrs11540947 (NM_000701: c.-78C > T) is located in the 5′UTR of *ATP1A1*. The schematic diagram of recombinant plasmid construction was shown as Supplemental Fig. 1A. The genomic DNA with genotype CC of rs11540947, as identified by Sanger sequencing, was selected as the template. The 5′UTR region of *hATP1A1* (+1-+339, the transcription start site (TSS) was set as +1 and rs11540947 was at +262) was amplified with 2 × Phanta Max Master Mix (Vazyme, China). The *Kpn* I and *BgI* II restriction sites were designed at the 5′-end of forward and reverse primers, respectively. The purified target DNA was ligated into the pGL3-basic vector and then transfected into E.*coli* DH5α. The recombinant plasmids pGL3-hATP1A1-5′UTR-Wild were collected by using the TaKaRa MiniBEST Plasmid Purification Kit (Takara, China), followed by site-directed mutagenesis using the Takara MutanBEST kit. The sequences of the wild plasmid pGL3-hATP1A1-5′UTR-Wild and the mutated recombinant plasmid pGL3-hATP1A1-5′UTR-(+262) MUT were verified by Sanger sequencing (Supplemental Fig. 1B). The following primers were used:

hATP1A1 5′UTR forward: 5′-GGGGTACCGACGTTTCGCGGCGTGGG-3’ (*Kpn* I), *hATP1A1* 5′UTR reverse: 5′-GAAGATCTGGTGGCGGTGCTCAGT-3’ (*BgI* II); *hATP1A1* 5′UTR mutation forward: 5′-CCGCTCGCT***T***GGCCGGGAG -3′, *hATP1A1* 5′UTR mutation reverse: 5′-GACCAGGGGAGCCAAGTGG -3’.

2.7. Cell culture

The HEK293 and HK2 cells were cultured in Dulbecco’s modified Eagle medium (DMEM) supplemented with 10% fetal bovine serum and maintained at 37 °C in a 5% CO_2 atmosphere. HK2 cells were exposed to 100 μg/mL calcium oxalate monohydrate (COM) for 0, 3, 6, 12, 24, and 48 h [25]. Before 1 h of COM exposure to HK2, 1 μM tat-pNaktide and tat-scramble as well as 0.1–10 μM 5-aza-2′-deoxycytidine (5Aza-2dc) were added to the DMEM, respectively. pNaktide as a specific inhibitor for the ATP1A1/Src signaling complex and tat-scramble as a negative control, were designed as before and synthesized with purity >95% by ShangHai Science Peptide Biological Technology Co., LTD (Shanghai, China) [27]. 5Aza-2dc, a specific inhibitor of DNA methyltransferase, was purchased from Sigma, St Louis, MO, USA. The sequences of pNaktide and tat-scramble were as follows:

Tat-pNaKtide: Ac-GRKKRRQRRRPPQSATWLALSRIAGLCNRAVFQ-NH2; Tat-scramble: Ac-GRKKRRQRRRPPQLWRRQLAFAI-TALVCSNSAG-NH2.

2.8. Transient transfection and dual luciferase reporter assay

The HEK293 and HK2 cells were seeded into a 12-well plate. The recombinant plasmids pGL3-hATP1A1-5′UTR-Wild and pGL3-hATP1A1-5′UTR-(+262) MUT were transfected into cells for 48 h with Lipofectamine 2000 (Vazyme, China) according to the manufacturer’s protocol. The promoter activity was detected by using the Duo-Lite Luciferase Assay System (Vazyme, China). The pGL3-basic was used as the background control, and the plasmid containing renilla firefly reporter gene served as to normalize the results. All the experiments were performed three times independently.

2.9. Adenovirus infection

To overexpress ATP1A1, we constructed a recombinant adenovirus containing the whole coding sequence of human *ATP1A1* cDNA (NM_000701) and a red fluorescent protein mCherry, which was termed as HBAD-Adeasy-hATP1A1-3xflag-mCherry (Ad-hATP1A1). HBAD-mCherry served as a negative control adenovirus. HK2 cells were infected with Ad-hATP1A1 and HBAD-mCherry at 20 multiplicity of infection (MOI) for 48 h and then exposed to COM.

2.10. Detection of NKA activity

The activity of NKA in HK2 cells was detected with the Na/K-ATPase assay kit (Nanjing Jiancheng Bioengineering Institute, China) according to the manufacturer’s specification. The protein concentration was determined with the BCA protein assay kit (Solarbio, China). The activity of NKA was expressed as *U* per milligram protein.

2.11. Quantitative real time PCR (qRT- PCR)

1 μg of total RNA were extracted from HK2 cells or rat kidney tissues with the RNA isolator (Vazyme, China) and were reversed into cDNA with the HiScript II RT SupeMix (Vazyme, China). The qRT-PCR (40 cycles) was performed with the ChamQ Universal SYBR qPCR Master Mix (Vazyme, China) by using the Applied Biosystem 7500 fast Real-Time PCR instrument. The human *GADPH* and the rat *Actin* were used to normalize the mRNA levels of *ATP1A1*, *DNMT1*, *DNMT3A* and *DNMT3B*. The following primers were used:

human *ATP1A1* forward: 5′-GACGTGATAAGTATGAGCCTG-3′, human *ATP1A1* reverse: 5′-AATCCCCGGCTCAAGTCTGT-3’; human *DNMT1* forward: 5′-GGTTCTTCCTCCTGGAGAATGTC-3′, human *DNMT1* reverse: 5′-GTCTGGGCCACGCCGTACTG-3’; human *DNMT3A* forward: 5′-AGTTAGCAGCAGGGAGACGA-3′, human *DNMT3A* reverse: 5′-AAGAGGTAACAGCGGCTTCTA-3’; human *DNMT3B* forward: 5′-AGGGAAGACTCGATCCTCGTC-3′, human *DNMT3B* reverse: 5′-GTGTGTAGCTTAGCAGACTGG-3’; human *GAPDH* forward: 5′-CTTTGGTATCGTGGAAGGAC-3′, human *GAPDH* reverse: 5′-GAAATGAGCTTGACAAAGTG-3’; rat *Atp1a1* forward: 5′-TATCTGCAAATGGCTGCAAG-3′, rat *Atp1a1* reverse: 5′-CCCAGTGTACACAACGATGC-3’; rat *Actin* forward: 5′-AGCCATGTACGTAGCCATCC-3′, rat *Actin* reverse: 5′-TCTCAGCTGTGGTGGTGAAG-3’.

2.12. Western blotting analysis

Total proteins were extracted from HK2 cells and rat kidney tissues with the RIPA buffer (Solarbio, China). 20 μg protein lysates per well were separated by SDS-PAGE and transferred onto PVDF membranes. After blocked with 5% bovine serum albumin, the blots were incubated with the primary antibodies as follows: anti-phosphorylated Src^{Y418} (ab133460) and anti-Src (ab109381) were purchased from Abcam; phospho-SAPK/JNK (Thr183/Tyr185) rabbit monoclonal antibody (#4668), SAPK/JNK rabbit antibody (#9252), phospho-p38 MAPK (Thr180/Tyr182) mouse monoclonal antibody (#9216), p38 MAPK rabbit monoclonal antibody (#8690), and cleaved caspase 3 (Asp175) antibody (#9661) were purchased from Cell Signaling Technology (Beverly, MA); DNMT1(Cat:24206), DNMT3a (Cat:20954), and ATP1A1 (Cat:14418) rabbit polyclonal antibodies were purchased from Proteintech (Wuhan, China); DNMT3b rabbit polyclonal antibody (A2899) and β-Actin rabbit monoclonal antibody were purchased (AC026) from Abclonal (Wuhan, China). HRP goat anti-rabbit/mouse IgG (AS014/AS003) from Abclonal were used as the secondary antibodies. The relative expression of the proteins was calculated with the Image J software.

2.13. Measurement of intracellular ROS

The intracellular ROS level was detected with a ROS-sensitive fluorescent dye 2′, 7′-dichloroflfluorescin diacetate (DCFHDA; Molecular Probes), as described previously [28]. Briefly, the HK2 cells were seeded onto glass coverslips and incubated with 20 μM DCFHDA in PBS at 37 °C for 30 min. The antifade mounting medium with DAPI (Beyotime, China) was used to stain the nucleus. The resultant fluorescence was captured by fluorescence microscopy (Olympus, Japan). Image J software was used to determine the fluorescent intensity.

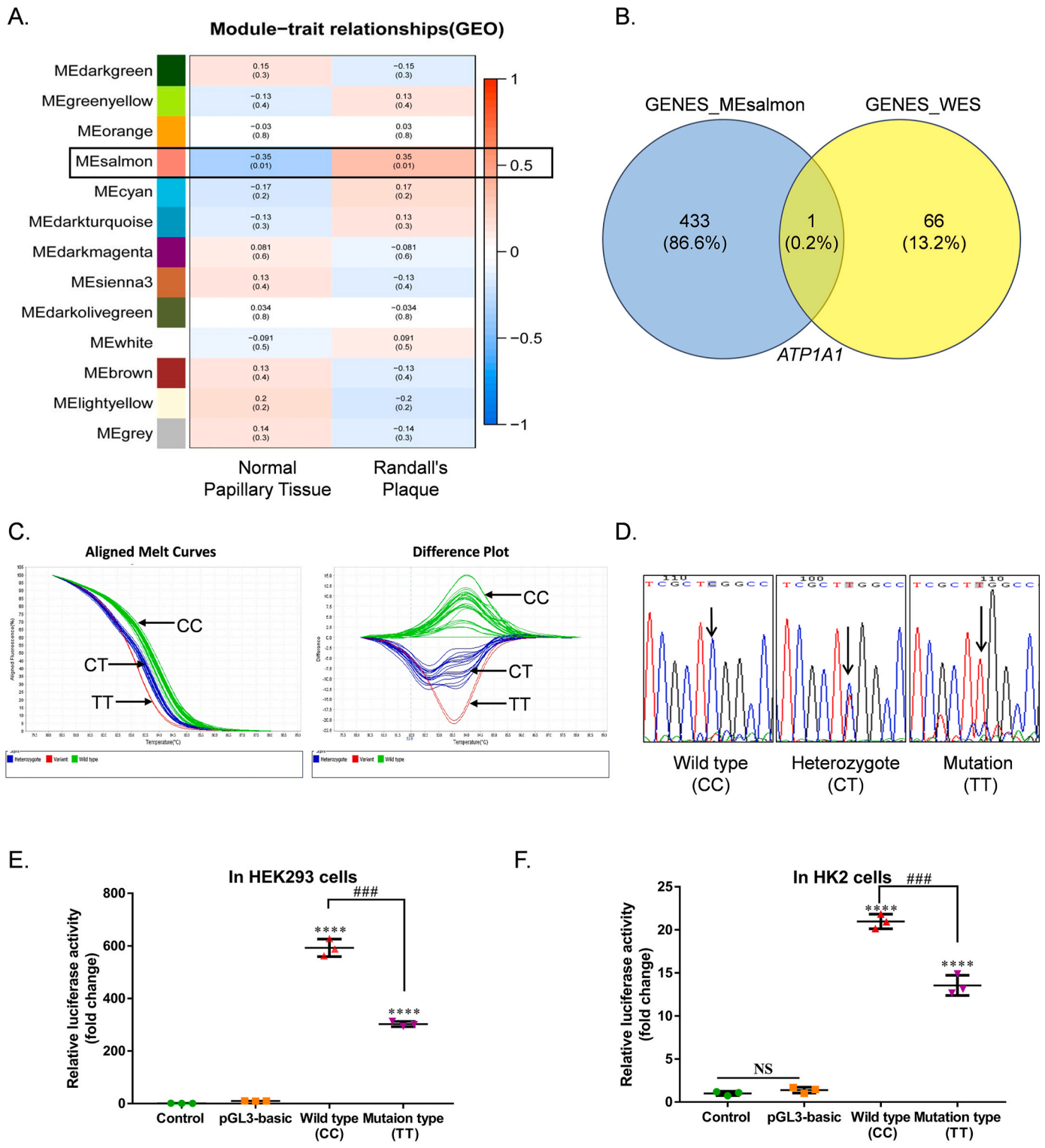

Fig. 1. Investigation of the association of *ATP1A1* genetic variation with CaOx stone through integration analysis of the gene expression profiles of GSE73680 and the WES data. (A) WGCNA analysis for 52 samples of P group (n = 27) and N group (n = 25) from GSE73680. The salmon module was identified to be related to calcium stone ($p = 0.01$). (B) *ATP1A1* was identified by Venn diagram analysis for the genes obtained from the salmon module (434 genes) and the candidate genes from the WES data (67 genes). (C) SNPrs11540947 (NM_000701: c.-78C > T) was genotyped with HRM. Each sample was tested at least thrice, independently. The results were determined by the aligned melt curves (the left panel) and the difference plots (the right panel). Three genotypes were identified (CC: green; CT: blue; TT: red). (D) Sanger sequencing was performed for rs11540947 in *ATP1A1*, which is indicated with black arrows. (E–F) The allele difference of rs11540947 in the promoter activity of *ATP1A1* was detected by the dual-luciferase reporting system in HEK293 cells (E) and HK2 cells (F). The relative luciferase activity was calculated as the fold change relative to the control group. Three independent experiments were performed, and the values are expressed as the mean ± SD (n = 3). ****$p < 0.0001$ vs. pGL3-basic; ###$p < 0.001$ vs. the wild-type (CC). (For interpretation of the references to color in this figure legend, the reader is referred to the Web version of this article.)

Table 1
GO and KEGG analysis for the 434 genes in the salmon modules.

Term	Count	%	*p* Value	Benjamini	FDR
GOTERM_BP_DIRECT					
GO:0048704~embryonic skeletal system morphogenesis	14	3.6553	1.96E-13	3.77E-10	3.75E-10
GO:0009952~anterior/posterior pattern specification	15	3.9164	1.16E-09	1.12E-06	1.11E-06
GO:0035725~sodium ion transmembrane transport	10	2.6110	6.71E-05	0.04311	0.04295
GO:0034220~ion transmembrane transport	14	3.6553	1.07E-04	0.04361	0.04346
GO:1990573~potassium ion import across plasma membrane	7	1.8277	1.13E-04	0.04361	0.04345
GOTERM_CC_DIRECT					
GO:0070062~extracellular exosome	84	21.9321	5.33E-11	2.04E-08	2.01E-08
GO:0016324~apical plasma membrane	25	6.5274	6.80E-08	1.30E-05	1.28E-05
GO:0005887~integral component of plasma membrane	56	14.6214	1.07E-07	1.37E-05	1.34E-05
GO:0016323~basolateral plasma membrane	19	4.9608	2.52E-07	2.29E-05	2.24E-05
GO:0016021~integral component of membrane	142	37.0757	2.98E-07	2.29E-05	2.24E-05
GO:0005886~plasma membrane	125	32.6371	2.35E-05	0.0015	0.0015
GO:0005890~sodium:potassium-exchanging ATPase complex	5	1.3055	4.56E-05	0.0025	0.0025
GO:0000785~chromatin	35	9.1384	4.54E-04	0.0217	0.0213
GO:0016020~membrane	68	17.7546	5.86E-04	0.0249	0.0245
GOTERM_MF_DIRECT					
GO:0004867~serine-type endopeptidase inhibitor activity	10	2.6109	1.44E-04	0.08448	0.08448
KEGG_PATHWAY					
hsa01100:Metabolic pathways	52	13.5770	3.52E-05	0.0076	0.0074
hsa04960:Aldosterone-regulated sodium reabsorption	7	1.8277	7.00E-05	0.0076	0.0074
hsa04978:Mineral absorption	8	2.0888	1.51E-04	0.0109	0.0106
hsa04961:Endocrine and other factor-regulated calcium reabsorption	7	1.8277	5.35E-04	0.0289	0.0282
hsa04974:Protein digestion and absorption	9	2.3499	8.61E-04	0.0331	0.0323
hsa04964:Proximal tubule bicarbonate reclamation	5	1.3055	9.19E-04	0.0331	0.0323
hsa04512:ECM-receptor interaction	8	2.0888	0.001577	0.0487	0.0475

2.14. Apoptosis detection

Apoptosis was detected with the Annexin V-FITC apoptosis detection Kit (Vazyme, China) according to the manufacturer's instruction. Briefly, the cells on glass coverslips were fixed with 4% polyoxymethylene and then incubated with the Annexin V-FITC for 10 min in dark, which was followed by incubation with the antifade mounting medium with DAPI (Beyotime, China). The images were taken with the fluorescence microscopy. The apoptosis rate was calculated as the percentage of the apoptotic cells to the adherent cells.

2.15. Atomic absorption assay

To analyze the crystal adhesion on the cell surface, atomic absorption was performed as described previously [25]. Briefly, the cells were treated with 100 μg/mL of COM crystals for 5 min. The non-adherent crystals were removed by washing the cells thrice with PBS. The adherent crystals were collected in 6 M HCl and quantified by measuring the calcium concentration in the supernatants through atomic absorption analyses.

2.16. Animal models

A total of 49 male Sprague–Dawley (SD) rats (age: 5–6 weeks old, weight: 150 ± 10 g) were randomly categorized into the following five groups: the negative control (−) group (n = 9), the blank control group (n = 10), the pNaKtide group (n = 10), the scramble group (n = 10), and the 5Aza-2dc group (n = 10). The rats in the (−) group received natural water, while those in the other 4 groups had free access to water supplemented with 2 g/L calcium and 20 g/L hydroxyproline (HYP) aimed to induce a CaOx stone model, as described previously [29]. pNaKtide administration was modified according to the pharmacological experimental methodology and a previous study [30]. 5Aza-2dc treatment was designed according to a previous study [31]. pNaktide and tat-scramble at a dose of 17.5 mg/kg, and 5Aza-2dc at a dose of 1 mg/kg, were dissolved in 0.9% saline and intraperitoneally injected into the experimental rats at every 48 h. In contrast, the rats in the blank control group received only 0.9% saline in the same manner. Three rats were dissected at 0 weeks, the time before inducing the CaOx stone model. At 2 weeks and 4 weeks, 23 rats were dissected, which included three rats in the (−) group and five rats in each of the other four groups. All protocols of rat experiments were approved by the Shenyang Medical College Animal Committee.

2.17. HE staining

Kidney tissues in the (−) group, the blank control group, the scramble group, and the pNaKtide group (total 39 rats) were fixed with 4% polyoxymethylene and cut into 5 μm thick paraffin sections, which were stained with hematoxylin and eosin.

2.18. Immunohistochemistry (IHC)

Immunohistochemical staining was performed on the rats at 0 weeks (n = 3) and on the rats in the blank control group who received HYP + $CaCl_2$ for 2 weeks and 4 weeks (n = 5 per time point). After dewaxing, antigen repair, treatment with 3% hydrogen peroxide and blocking with goat serum, the rat kidney slice was incubated with ATP1A1 rabbit polyclonal antibody (Proteintech, China), followed by treatment with HRP goat anti-rabbit IgG (Abclonal, China). The relevant images were captured with an optical microscope (Olympus, Japan).

2.19. Measurement of urine oxalate excretion

The rats in the (−) group, the blank control group, the scramble group, and the pNaKtide group were subjected to urine oxalate detection analyses. For this purpose, urine samples were collected in metabolic cages for 24 h the day before the rats were dissected. After decolorization, the concentration of urine oxalate was determined by using the oxalate content assay kit (Solarbio, China), according to the manufacturer's specifications.

2.20. Statistical analysis

Statistical analysis was performed by utilizing the GraphPad Prism 7.0 software. Statistical comparisons for allele distribution and genotype distribution between the controls and cases were analyzed with the Chi-square test. To determine the risk of kidney stones for a given allele, the

Table 2
List of 67 candidate genes and the corresponding 76 SNPs identified from the WES data of 28 patients with CaOx stone.

Gene symbol	SNPs
OR52E4	rs4758168
OR5AK2	rs2853083
MCCD1	rs3093983, rs3093979
BAT1	rs2239528
C6orf91	rs1529151
AADAC	rs1803155
KCNC4	rs59123361
ZPBP	rs61696422
ZFR	rs4867440
RADLL	rs6966329
RFWD3	rs8058922
L1TD1	rs7533274, rs7551777
KIAA1217	rs10828663
NLRX1	rs4245191
PDZD3	rs1815811
PIF1	rs17802279
BRWD1	rs2183573
SIGLEC12	rs2034891
PTPRN2	rs3800855
C6orf150	rs9352000, rs9446904
MGC24039	rs1056320
WDR31	rs41307479
ACOT11	rs2304305
C1orf65	rs10907376
RPP38	rs7896053
B4GALNT3	rs11063529, rs1056008
KRT40	rs17843015
NAV2	rs6483617
PRUNE2	rs683866
R3HCC1	rs3808536, rs2272761, rs13530
FBN1	rs363830, rs363836
PON3	rs363836
PARVB	rs738479
NWD1	rs773852
CYP11B1	rs34570566
TTC23	rs2602016
TMPRSS13	rs59590191
TMEM202	rs35916586
ADPRH	rs20569
GNAI1	rs10241877
PRKCA	rs2228945
ROS1	rs3752564
RASSF7	rs34954482, rs7109278
DCLK1	rs2322807
RBM6	rs2023953
KLF13	rs11537749
CECR1	rs7289141
RNF20	rs10521057
SLC22A23	rs9503518
QRICH2	rs347675
ANKRD30A	rs57914746
HDGFL1	rs6922960
MASP1	rs850312
ATP1A3	rs2217342
SIGLEC6	rs1993462, rs12609761
ANKRD13D	rs2298815
AK1	rs4226
HLA-DOB	rs2070120
SEMA4G	rs11591349
FIBCD1	rs11792889
UBASH3B	rs1540108
GUK1	rs4653908
ATP1A1	rs11540947
UNC50	rs1062847
RINT1	rs818620
PSMAL	rs10830330
OSGIN1	rs58056773

odds ratio (OR) and 95% confidence interval (CI) were accordingly calculated. For other experiments, each experiment consisted of at least three independent replicates and all the values were expressed as the mean ± SD or SEM. Two groups of normally distributed variables were compared using an unpaired Student's *t*-test, whereas two groups of not-normally distributed variables were compared using the Mann–Whitney *U* test. The two-way ANOVA analysis of variance was performed to compare the different levels of two factors. $p < 0.05$ was considered to indicate statistical significance.

3. Results

3.1. Integrated analysis of the gene expression profiles and WES data of calcium stones patients suggested that ATP1A1 may be a crucial gene related to nephrolithiasis

After data evaluation, four abnormal samples (i.e., GSM1900696, GSM1900697, GSM1900699, and GSM1900726) in the N group and P group from GSE73680 were excluded. The remaining 52 samples were analyzed with WGCNA. A total of 13 modules were identified (Fig. 1A), among which only the salmon module was found to be associated with calcium stones ($p = 0.01$). A total of 434 genes (Supplemental Table 1) were extracted from the salmon module for GO and KEGG analyses, with $p < 0.05$ and FDR < 0.1 (Table 1), showing that these genes were enriched in the plasma membrane and the transmembrane transport (GO analysis). The KEGG enrichment analysis revealed that these genes were involved in "Aldosterone-regulated sodium reabsorption", "Mineral absorption", "Endocrine and other factor-regulated calcium reabsorption", and "Proximal tubule bicarbonate reclamation". Cumulatively, we discovered that five genes encoding NKA, including *FXYD2*, *FXYD4*, *ATP1A4*, *ATP1A1*, and *ATP1B1*, participated in the processes of transmembrane transport, absorption, and reabsorption. These results suggested that NKA may be closely related to nephrolithiasis.

To further explore the key genes involved in nephrolithiasis, the WES of 28 CaOx stone patients from Chinese Han people was performed. A total of 76 SNPs with $p < 0.005$, including 31 missense SNPs, 30 coding-synonymous SNPs, 7 SNPs in the 3′ untranslated region (UTR), and 8 SNPs in the 5′UTR, were obtained and listed as candidate SNPs, which were then mapped to 67 genes (Table 2).

Next, we integrated the 434 genes in the salmon module with the 67 genes from WES data for Venn diagram analysis and found that *ATP1A1* was the only gene in the intersection of the two data sets (Fig. 1B), implying the potential role of *ATP1A1* in calcium stone formation.

3.2. T-allele of rs11540947 in the 5′UTR of ATP1A1 was associated with a high risk of calcium stones and a lower promoter activity of ATP1A1

We next extracted the SNP of *ATP1A1* from the WES data (Table 3). The frequency of the T-allele of rs11540947 in cases was 16.1%, while that in the control was 2.4% ($p = 0.0037$). To further confirm the correlation between rs11540947 and calcium stone formation, 214 patients with calcium stone and 232 matching controls were collected to detect the genotype of rs11540947 by HRM analysis (Fig. 1C). The results of DNA sequencing revealed complete consistency with the HRM results (Fig. 1D), emphasizing the validity of HRM genotyping. Statistical results (Table 4) revealed that carriers with CT + TT were more common in patients than that in controls ($p = 0.0324$, 95% CI 1.034–2.467). Similarly, the T-allele frequency in cases was greater than that in the controls ($p = 0.0311$, 95% CI 1.034–2.277). In terms of gender, rs11540947 was found to be remarkably associated with the risk of calcium stones in men, but there was no significant correlation in women. Together, these data suggested that the T-allele of rs11540947 was associated with a higher risk of calcium stones.

SNPrs11540947 (NM_000701: c.-78C > T) was located in the 5′UTR of human *ATP1A1*; this region may exhibit a promoter activity in its corresponding DNA sequence [32–34]. An Sp1-binding site and a potential TATA box were identified in the 5′UTR of *ATP1A1*, implying promoter activity in the 5′UTR [35]. Therefore, we analyzed whether rs11540947 yielded allelic differences in *ATP1A1* transcription. The dual-luciferase reporter assay revealed that, on the transfection with

Table 3
Whole exome sequencing analysis for rs11540947 (C > T) in *ATP1A1*.

Chromosome	Name	Assoc Allele	Case, Control Ratio Counts	Case, Control Frequencies	Chi square	*p* value	feature	gene
1	rs11540947	T	9:47, 2:80	0.161, 0.024	8.43	0.0037	5′-UTR	*ATP1A1*

The 41 controls (82 alleles) were from the 1000 Genomes Project database.

Table 4
Association analysis of carriers of the T-allele of SNPrs11540947(C > T) in 214 cases and 232 controls.

	SNPrs11540947	No. Cases (%)	No. Controls (%)	OR (95%CI)	Chi-Square	*p* value
All	Genotype					
	CC	152 (71.03)	185 (79.74)	1.606 (1.034–2.467)	4.577	0.0324*
	CT + TT	62 (28.97)	47 (20.26)	–	–	–
	Allele					
	C	361 (84.35)	414 (89.22)	1.537 (1.034–2.277)	4.649	0.0311*
	T	67 (15.65)	50 (10.78)	–	–	–
Male	Genotype					
	CC	102 (71.33)	118 (83.10)	1.976 (1.117–3.541)	5.606	0.0179*
	CT + TT	41 (28.67)	24 (16.9)	–	–	–
	Allele					
	C	242 (84.62)	257 (90.49)	1.731 (1.056–2.87)	4.514	0.0336*
	T	44 (15.38)	27 (9.51)	–	–	–
Female	Genotype					
	CC	50 (70.42)	67 (74.44)	1.223 (0.6024–2.459)	0.3233	0.5697
	CT + TT	21 (29.58)	23 (25.56)	–	–	–
	Allele					
	C	119 (83.80)	157 (87.22)	1.319 (0.7068–2.461)	0.758	0.3840
	T	23 (16.20)	23 (12.78)	–	–	–

*$p < 0.05$.
OR (95% CI) of genotype calculated as CC:(CT + TT).

pGL3-ATP1A1-5′UTR-wild (CC), HEK293 cells produced a stronger luciferase activity than the non-transfected cells and the pGL3-basic transfected cells, implying that the 5′UTR of *ATP1A1* exhibited a promoter activity (Fig. 1E). However, the transfection with pGL3-ATP1A1-5′UTR-(+262) MUT (TT) distinctly decreased the luciferase activity, suggesting that T-allele of rs11540947 mediated a significant reduction in the promoter activity of *ATP1A1*, which may decrease the expression of *ATP1A1* at the transcription level. The data obtained from HK2 cells revealed similar outcomes (Fig. 1F).

These results demonstrated that the genetic variation of *ATP1A1* at rs11540947 may play an important role in calcium stone formation by affecting the expression of ATP1A1.

3.3. COM exposure to HK2 cells activated the ATP1a1/src/ROS/MAPKs/NF-κB signaling pathway by inhibiting the ATP1A1 expression

Next, we examined the effects of COM exposure to HK2 cells on the activity of NKA and the expression of ATP1A1. Our results revealed that the NKA enzymatic activity and the *ATP1A1* mRNA level decreased dramatically 3 h after the COM treatment (Fig. 2A and B), while the protein level of ATP1A1 increased at 6 h after COM stimulation, followed by a reduction (Fig. 2C). With the change of ATP1A1 protein, the phosphorylation levels of Src also changed, demonstrating an evident activation 6 h after the COM exposure. Meanwhile, the oxidative stress-related signals p38 and JNK as well as the inflammation regulator NF-κB, including p65 and p50, were also activated. Nrf2, a key factor involved in anti-inflammatory and pro-survival processes [36], revealed a sharp upregulation at 3 h after the COM stimulation, followed by a decrease from 6 h to 48 h (Fig. 2C). ROS is an upstream signal for p38/JNK and NF-κB, and ROS accumulation induced by the activation of ATP1A1/Src has been identified in several diseases [15,16]. Here, we noted a significant increase in the intracellular ROS level after the COM exposure (Fig. 2D and E), which is possibly associated with the activation of the ATP1A1/Src signaling pathway.

In order to verify whether COM-induced Src/ROS/MAPKs/NF-κB signaling pathway activation was caused by the ATP1A1 protein decline, we constructed the recombinant adenovirus Ad-hATP1A1 to overexpress ATP1A1, using HBAD-mCherry as the negative control. The observation of red fluorescence in cells (Supplemental Fig. 2) and the western blotting results (Fig. 3A) demonstrated the successful overexpression of ATP1A1 driven by recombinant adenovirus. When compared to the HBAD-mCherry group, ATP1A1 overexpression inhibited the COM-induced activation of Src, p38, JNK, p65, and p50, as well as the decrease in Nrf2 (Fig. 3A). Moreover, the increased ROS level induced by COM was inhibited by Ad-ATP1A1 infection (Fig. 3B and C).

These data together demonstrated that COM exposure activated the ATP1A1/Src/ROS/MAPKs/NF-κB signaling pathway by reducing the ATP1A1 expression.

3.4. pNaKtide attenuated COM-induced oxidative stress and inflammation by inhibiting the ATP1A1/Src signaling pathway

To further investigate the effect of the ATP1A1/Src signaling pathway on oxidative stress and inflammation induced by COM, we used pNaKtide, a specific antagonist of the ATP1A1/Src signal complex, to inhibit the activation of Src [13]. The FITC-labeled pNaKtide displayed a successful distribution on the cell membrane (Supplemental Fig. 3). Western blotting analysis revealed that pNaKtide inhibited the activation of Src, p38, JNK, p65, and p50, as well as the decrease in Nrf2 when compared to those in the tat-scramble group (Fig. 4A); these results are consistent with those of ATP1A1 overexpression. As expected, pNaKtide successfully inhibited the accumulation of ROS induced by COM stimulation, thereby alleviating the intracellular oxidative environment (Fig. 4B and C).

3.5. ATP1A1 overexpression and pNaKtide treatment suppressed caspase 3-dependent apoptosis induced by COM and attenuated crystal-cell adhesion

Excessive oxidative stress can induce apoptosis. Here, we examined the effects of ATP1A1 overexpression and pNaKtide on COM-induced cell injury, and our results revealed that both reduced the COM-

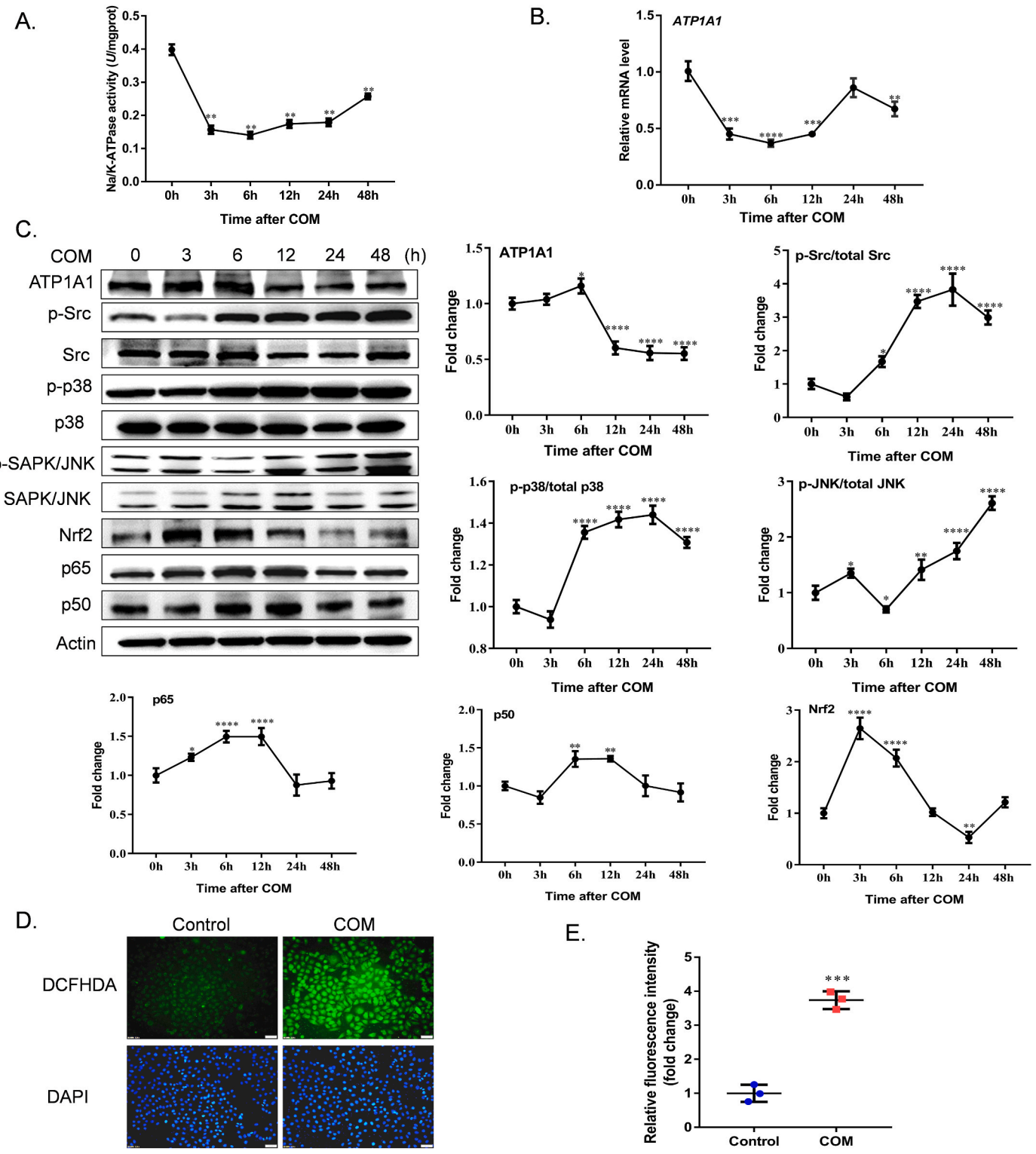

Fig. 2. COM exposure to HK2 cells activated the ATP1A1/Src/ROS/MAPKs/NF-κB signaling pathway. HK2 cells were exposed to 100 μg/mL COM for 0, 3, 6, 12, 24, and 48 h. Each experiment was independently repeated at least thrice. (A) The activity of NKA in HK2 cells decreased after COM stimulation. The data were expressed as the mean ± SD (n = 5). $^{**}p < 0.01$ vs. levels at 0 h. (B) COM exposure to HK2 cells inhibited the mRNA level of *ATP1A1*. The data were expressed as the mean ± SEM (n = 3). $^{**}p < 0.01$; $^{***}p < 0.001$; $^{****}p < 0.0001$ vs. levels at 0 h. (C) Western blotting analysis for the expressions of ATP1A1, p65, p50, Nrf2, and the phosphorylation of Src, p38, and JNK after COM exposure. The relative levels of proteins were calculated as a fold change relative to the level at 0 h. The data were expressed as the mean ± SD (n = 3). $^{*}p < 0.05$; $^{**}p < 0.01$; $^{****}p < 0.0001$ vs. the level at 0 h. (D–E) HK2 cells were exposed to 100 μg/mL COM for 24 h. Intracellular ROS was detected with a green fluorescent probe DCFHDA. The nuclei were stained with DAPI (blue). Scale bar = 50 μm. The relative fluorescence intensity was calculated as the fold change relative to the control group. The data were expressed as the mean ± SD (n = 3). $^{***}p < 0.001$ vs. the control. (For interpretation of the references to color in this figure legend, the reader is referred to the Web version of this article.)

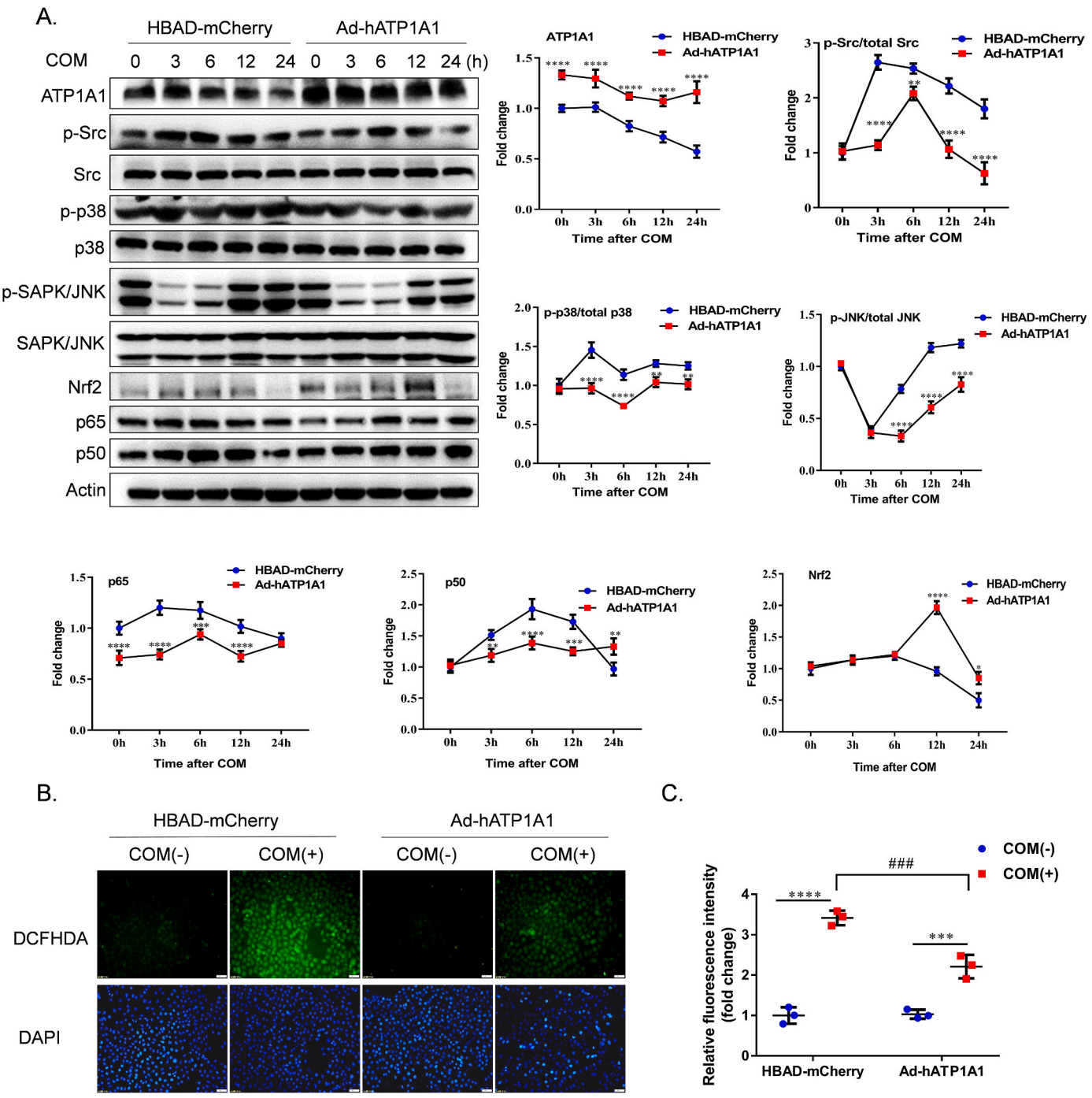

Fig. 3. ATP1A1 overexpression inhibited the activation of the ATP1A1/Src/ROS/MAPKs/NF-κB signaling pathway induced by COM exposure. HK2 cells were infected with Ad-hATP1A1 and HBAD-mCherry at 20 MOI for 48 h and then exposed to 100 μg/mL COM for 0, 3, 6, 12, and 24 h. Each experiment was repeated thrice, independently. (A) Western blotting analyzed the effects of ATP1A1 overexpression on the activation of Src, p38, JNK, p65, p50, and Nrf2. The protein levels were calculated as fold changes relative to the level at 0 h in the HBAD-mCherry group. The values were expressed as the mean ± SD (n = 3). $^{*}p < 0.05$; $^{**}p < 0.01$; $^{***}p < 0.001$; $^{****}p < 0.0001$ vs. levels in the HBAD-mCherry group. (B–C) HK2 cells infected with Ad-ATP1A1 and HBAD-mCherrry were exposed to 100 μg/mL COM for 24 h. Intracellular ROS was then measured with DCFHDA. Scale bar = 50 μm. The relative fluorescence intensity was calculated as fold changes relative to the level in the HBAD-mCherry group without COM treatment. The values were expressed as the mean ± SD (n = 3). $^{****}p < 0.0001$; $^{***}p < 0.001$ vs. COM (−). $^{\#\#\#}p < 0.001$ vs. the HBAD-mCherry group.

induced apoptosis when compared to the corresponding controls (Fig. 5A and B). Western blotting results (Fig. 5C and D) implied that COM-activated caspase 3 was significantly inhibited by ATP1A1 overexpression and pNaKtide, thereby blocking the process of apoptosis.

Crystal-cell adhesion is a crucial process involved in stone formation, and crystal deposition can damage renal cells [37,38]. Hence, we examined the role of ATP1A1 in crystal-cell adhesion. We observed significantly lower Ca^{2+} concentrations in both the groups after infection with Ad-hATP1A1 and treatment with pNaKtide, relative to the corresponding controls (Fig. 5E and F), suggesting that the ATP1A1 overexpression and pNaKtide could prevent crystal-cell adhesion, thereby protecting the cells from CaOx crystal-induced injury and decreasing the formation of kidney stones.

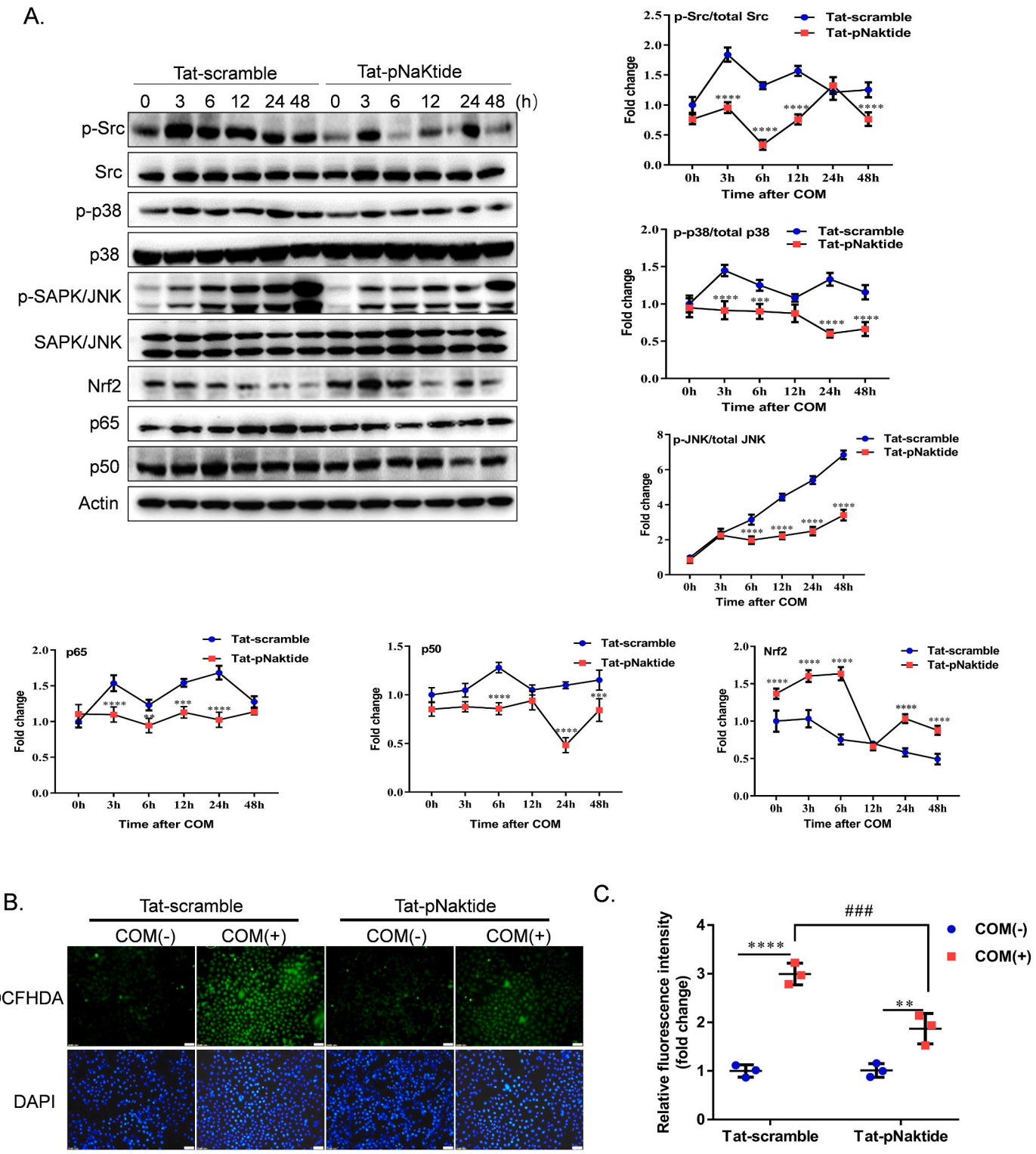

Fig. 4. pNaKtide attenuated ROS accumulation and inflammation induced by COM by inhibiting the ATP1A1/Src signaling pathway. HK2 cells were pretreated with 1 μM tat-pNaktide and tat-scramble, and then exposed to100 μg/mL COM for 0, 3, 6, 12, 24, and 48 h. Each experiment was independently repeated thrice. (A) Western blotting results revealed pNaKtide inhibited the activation of Src, p38, JNK, p65, and p50 while promoting the Nrf2 expression. The levels of these proteins were expressed as fold changes relative to the level at 0 h in the tat-scramble group. The values were expressed as the mean ± SD (n = 3). ***$p < 0.001$; ****$p < 0.0001$ vs. levels in the tat-scramble group. (B–C) After 24 h of COM exposure, pNaKtide decreased the intracellular ROS levels. Scale bar = 50 μm. The level of intracellular ROS was calculated as fold changes relative to the level in the tat-scramble group without COM treatment. The values were expressed as the mean ± SD (n = 3). **$p < 0.01$; ****$p < 0.0001$ vs. COM (−). ###$p < 0.001$ vs. the tat-scramble group.

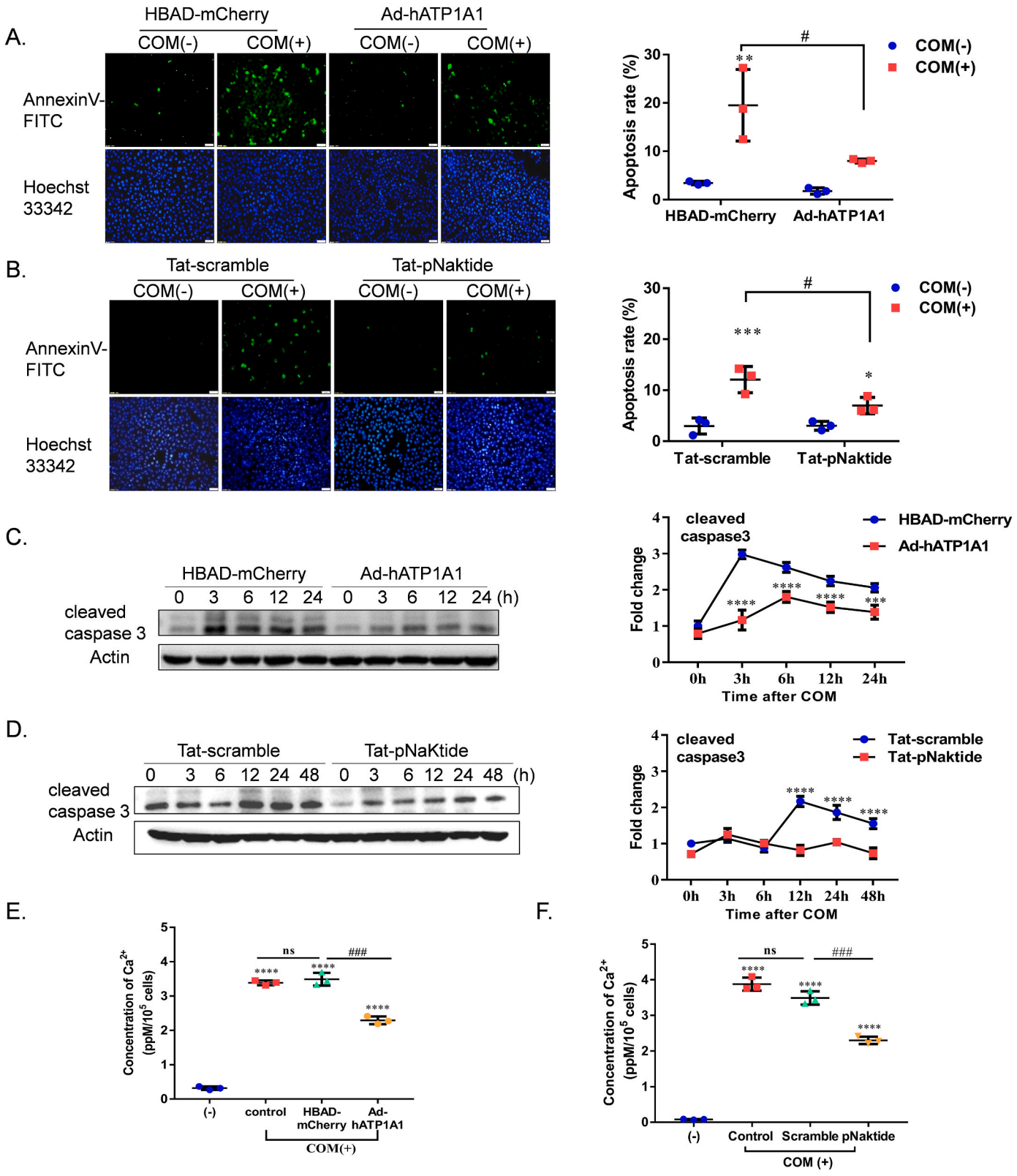

Fig. 5. ATP1A1 overexpression and pNaKtide treatment suppressed COM-induced apoptosis and attenuated crystal-cell adhesion. Each experiment was tested thrice, independently. (A–B) Apoptosis of Ad-hATP1A1 infected and pNaKtide-treated cells measured after 24 h of exposure to COM. Scale bar = 50 μM. The apoptosis rate was calculated as the percentage of apoptotic cells to the total adherent cells. The values were expressed as the mean ± SD (n = 3). *$p < 0.05$; **$p < 0.01$; ***$p < 0.001$ vs. COM (−). #$p < 0.05$ vs. the HBAD-mCherry group or the tat-scramble group. (C–D). Cleaved caspase 3 in Ad-hATP1A1 infected and pNaKtide-treated cells as measured by Western blotting after 24 h of exposure to COM. The values were expressed as the mean ± SD (n = 3). ***$p < 0.001$; ****$p < 0.0001$ vs. the HBAD-mCherry group or the tat-scramble group. (E–F) Crystal deposition on cells was investigated after infection with Ad-hATP1A1 or treatment with pNaKtide. (−) represents no adenovirus and no COM exposure. Control represents only COM exposure. The values were expressed as the mean ± SD (n = 3). ****$p < 0.0001$ vs. the (−) group. ###$p < 0.001$ vs. the HBAD-mCherry group or the scramble group.

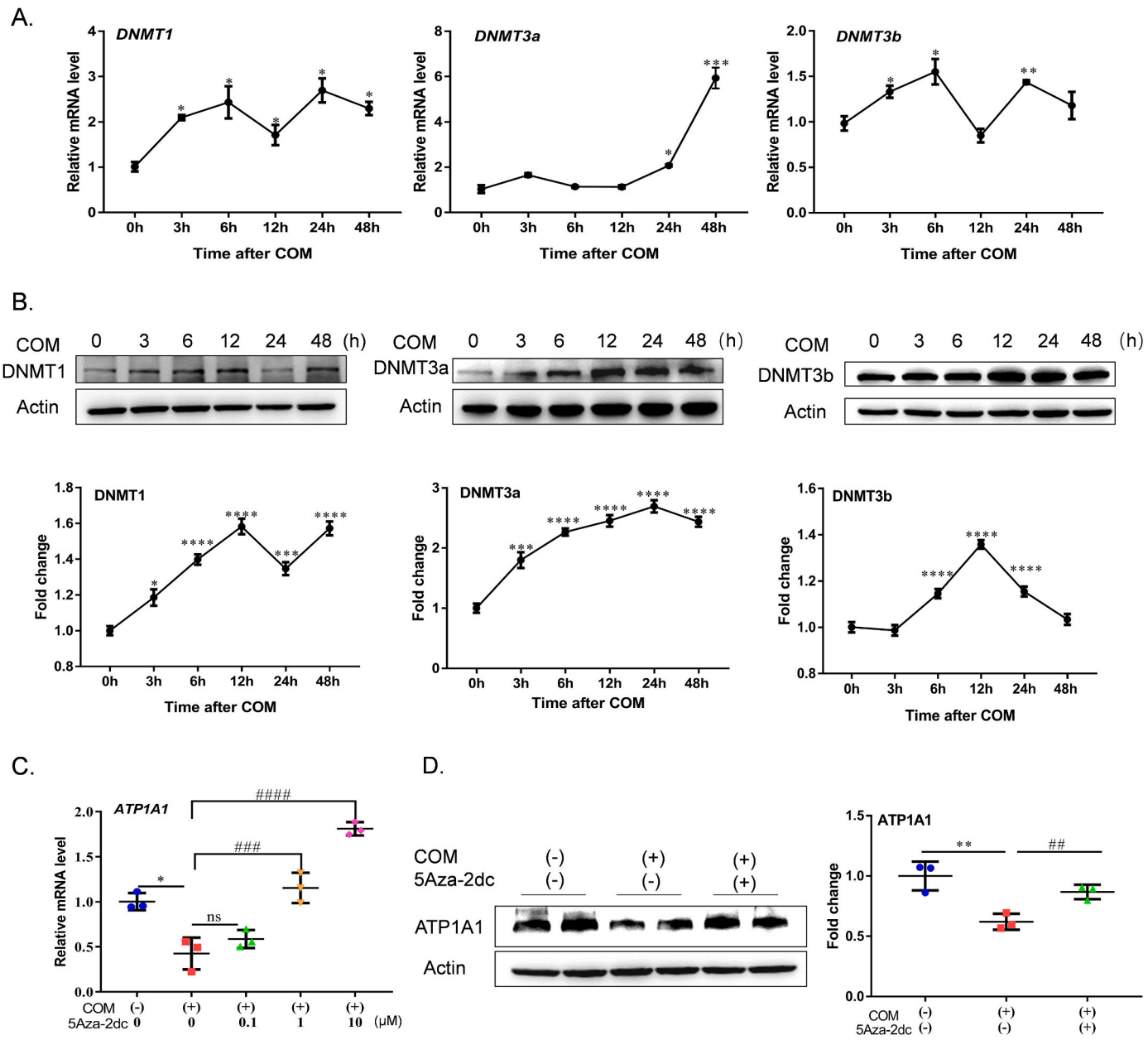

Fig. 6. DNA methylation participated in the downregulation of ATP1A1 induced by COM. (A) After exposing 100 μg/mL COM to HK2 cells, the mRNA levels of *DNMT1*, *DNMT3a*, and *DNMT3b*, were measured by qRT-PCR. The values were expressed as the mean ± SEM (n = 4). *$p < 0.05$; **$p < 0.01$; ***$p < 0.001$; vs. the levels at 0h. (B) The protein levels of DNMT1, DNMT3a, and DNMT3b were determined by Western blotting. The relative expression level was expressed as a fold change relative to the level at 0 h. Each experiment was repeated thrice, independently. The values were expressed as the mean ± SEM (n = 3). *$p < 0.05$; ***$p < 0.001$; ****$p < 0.0001$ vs. the levels at 0 h. (C) The *ATP1A1* mRNA level was detected after pretreatment with 5Aza-2dc, a specific inhibitor of DNA methyltransferase, at the concentration of 0.1–10 μM. The values were expressed as the mean ± SEM (n = 3). *$p < 0.05$ vs. COM (−); ###$p < 0.001$; ####$p < 0.0001$ vs. only COM (+). (D) The protein level of ATP1A1 was examined by Western blotting after pretreatment with 10 μM 5Aza-2dc. Three independent experiments were performed and the values were expressed as the mean ± SD (n = 3). **$p < 0.01$ vs. COM (−). ##$p < 0.01$ vs. only COM (+).

3.6. DNA methylation participated in the decrease of ATP1A1 induced by COM

The methylation of the CpG islands in the DNA promoter is a frequent mechanism involved in gene silencing [39], and *ATP1A1* is a housekeeping gene, as indicated by the presence of a CpG island [35]. Therefore, we investigated whether the COM-mediated ATP1A1 decrease was associated with DNA methylation. After COM exposure, both the mRNA and protein levels of DNA methyltransferases (DNMTs), including DNMT1, DNMT3a, and DNMT3b, were significantly increased (Fig. 6A and B). Then, the HK2 cells were pretreated with the DNA methylation inhibitor 5Aza-2dc before COM exposure, indicating an evident prevention in mRNA reduction of *ATP1A1* in a concentration-dependent manner (Fig. 6C). The protein level of ATP1A1 was also reversed by 5Aza-2dc after COM exposure (Fig. 6D). These results together suggested that altered DNA methylation participated in COM-induced ATP1A1 reduction.

3.7. pNaKtide inhibited crystal formation in vivo

To confirm the effect of ATP1A1 on crystal formation *in vivo*, the CaOx nephropathy rat model was constructed with SD rats who received water containing HYP and $CaCl_2$. The outline of the design of pNaKtide treatment for the CaOx stone rats is illustrated in Fig. 7A. When

compared with the (−) group, the HE staining revealed an obvious crystal deposition in the kidney after HYP and $CaCl_2$ treatment (Fig. 7B). Renal crystals were observed in 40% of the rats in the pNaKtide group and the crystal area observed in this group was significantly smaller than that observed in the control group (Fig. 7C). The 24-h urine sample testing also showed a significant decrease in urine oxalate excretion after treatment with pNaKtide (Fig. 7D). Similar to the *in vitro* study results, HYP + $CaCl_2$ treatment also decreased *ATP1A1* mRNA and

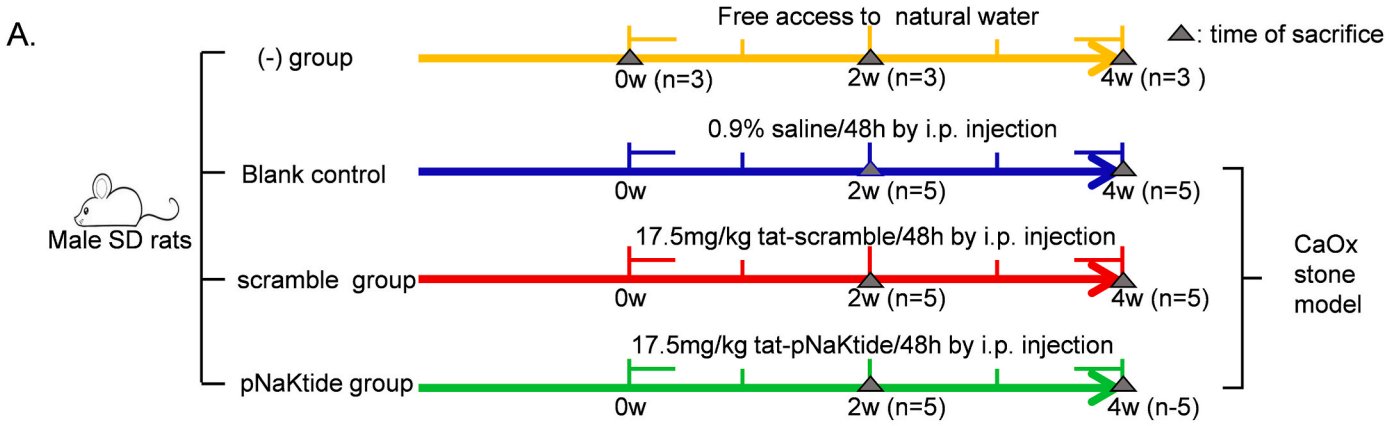

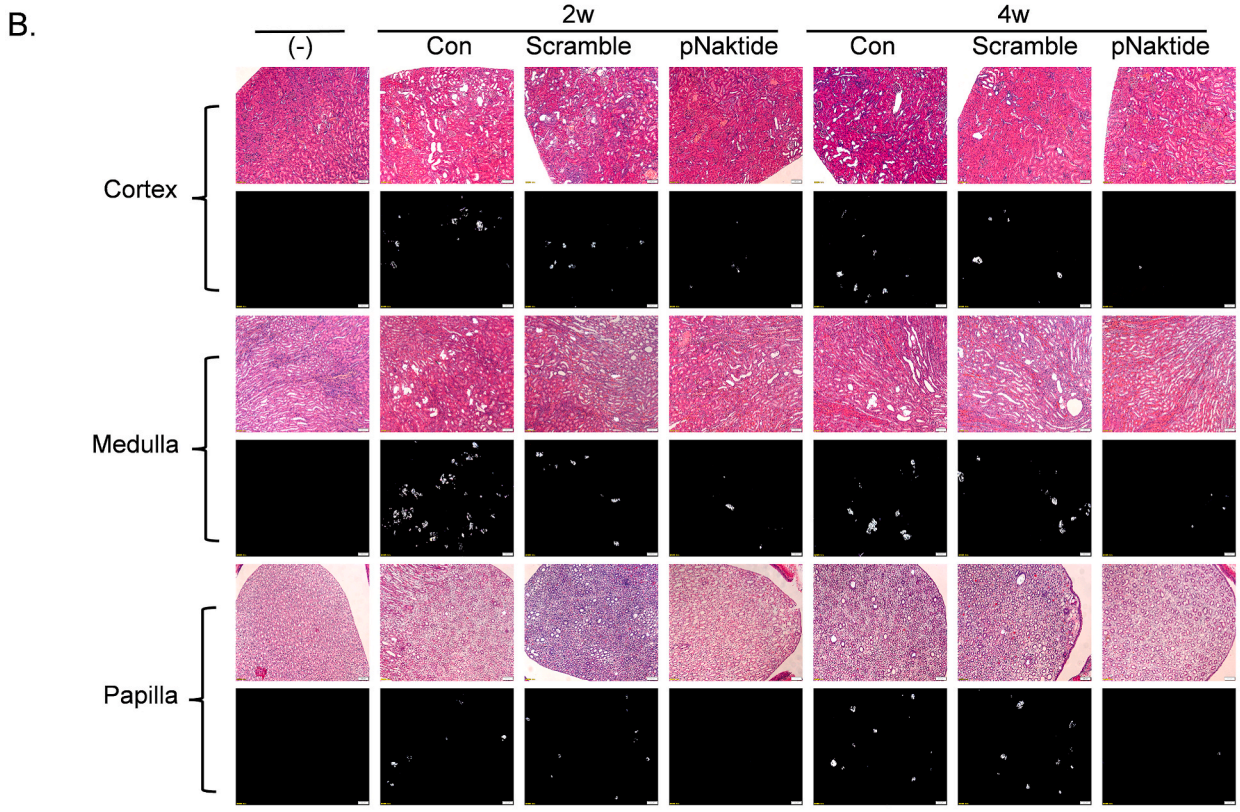

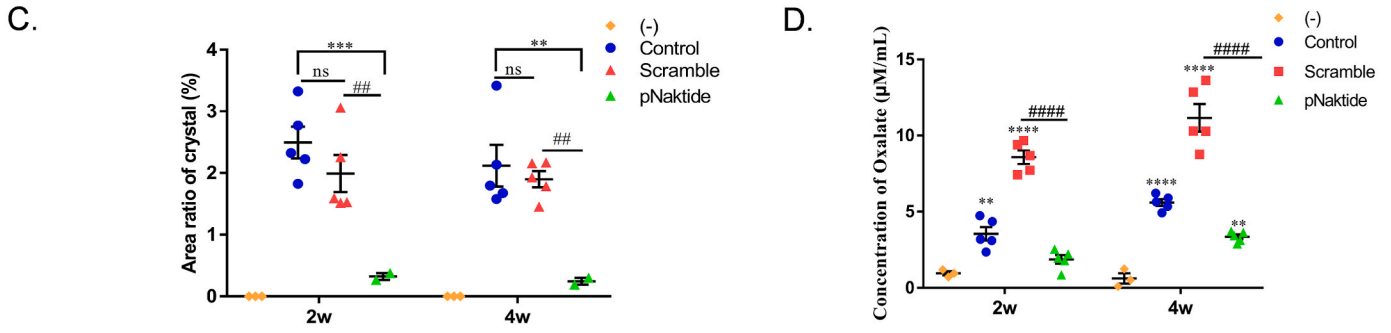

(caption on next page)

Fig. 7. pNaKtide inhibited crystal formation *in vivo*. (A) An outline of the design of pNaKtide treatment for CaOx stone rats. The CaOx stone rat models were induced by giving water containing 20 g/L HYP and 2 g/L $CaCl_2$. The (−) group represents rats that received free access to natural water for 2 and 4 weeks, respectively (n = 3 per time point). The blank control group represents the CaOx stone model rats that received water containing HYP + $CaCl_2$ for 2 and 4 weeks, which were simultaneously treated with 0.9% saline through intraperitoneal injection (i.p.) per 48 h (n = 5 per time point). The rats in the pNaKtide group and the scramble group also received water containing HYP + $CaCl_2$ for 2 and 4 weeks and were simultaneously treated with tat-pNaKtide and tat-scramble respectively, at a dose of 17.5 mg/kg per 48 h by i.p. injection (n = 5 per time point, n = 10 per group). The rats were sacrificed before treatment (0 weeks) and at the end of 2 weeks and 4 weeks. (B) The rats in the (−) group, the blank control group, the scramble group, and the pNaKtide group were dissected for histological observation of the kidney after HE staining (n = 9 in the (−) group, n = 10 in other three groups). The crystal in the rat kidney slice was captured under a polarizing microscope. Scale bar = 100 μM. (C) The area ratio of crystals in the rat kidney was calculated as the percentage of the crystal area to the total area. Only two rats in the pNaKtide group developed renal crystals. The values were expressed as the mean ± SEM (n = 2, 3, or 5). $^{**}p < 0.01$; $^{***}p < 0.0001$ vs. the control group; $\#\#p < 0.01$ vs. the tat-scramble group. (D) 24 h-urine was collected in metabolic cages to measure the urine oxalate excretion. The values were expressed as the mean ± SEM (n = 3 in the (−) group, n = 5 in other groups). $^{**}p < 0.01$; $^{****}p < 0.0001$ vs. the (−) group. $\#\#\#\#p < 0.0001$ vs. the tat-scramble group.

protein levels (Fig. 8A–D), activated Src, p38, JNK, p65, and p50, and decreased Nrf2 expression. All these phenomena were reversed by pNaKtide (Fig. 8E and F). Moreover, 5Aza-2dc inhibited ATP1A1 reduction induced by HYP + $CaCl_2$ treatment, indicating that ATP1A1 expression was regulated by DNA methylation *in vivo* (Fig. 8G and H). These *in vivo* results emphasized the importance of ATP1A1 and the ATP1A1/Src signaling pathway in kidney stone formation.

4. Discussion

Nephrolithiasis is a complex multifactorial disease with evident genetic predisposition and environmental influence. The identification of its susceptibility genes has been a challenge despite some progress made in this field. Here, we noted that *ATP1A1* may be a potentially crucial gene involved in kidney stone formation through integrated omics analysis. The T-allele of rs11540947 in 5′UTR of *ATP1A1* decreased the promoter activity and was associated with a higher risk of stone formation. Further studies both *in vitro* and *in vivo* showed that COM exposure could decrease the expression of ATP1A1 through altered DNA methylation, resulting in the activation of the ATP1A1/Src signaling pathway and ROS accumulation, which, in turn, caused NF-κB/Nrf2 inflammation and apoptosis through stress-related signals of p38 and JNK. The inhibition of ATP1A1/ROS by ATP1A1 overexpression or pNaKtide reduced COM-induced inflammation, apoptosis, and crystal-cell adhesion, thereby preventing the renal crystal formation (Fig. 9). These findings suggest new ideas and strategies to target ATP1A1 for the treatment of nephrolithiasis, at least CaOx stones.

RP is the anchoring site for calcium stones on kidney papillary surfaces. Understanding the molecular genetic mechanism of RP formation is crucial for developing targeted therapies against kidney stones. Therefore, Taguchi et al. investigated the gene expression profiles (GSE73680) of the RP section from human papillary tissues, and performed differentially expressed gene (DEG) analysis [23]. They found that compared with non-RP tissues, RP tissues showed the upregulation of *LCN2*, *IL11*, *PTGS1*, *GPX3*, and *MMD* (> 2-fold), and the downregulation of *SLC12A1* and *NALCN* (0.5-fold) ($p < 0.01$). These genes are associated with activated mitogen-activated protein kinase, the Akt/-phosphatidylinositol 3-kinase pathway, and proinflammatory cytokines that cause renal injury and oxidative stress [23]. DEGs are screened based on the absolute fold change threshold, the selection of which has certain limitations because of the gene expression abundance. Furthermore, it is greatly affected by the subjective choice of researchers, leading to the loss of some information. Conversely, WGCNA is a system biology method for identifying disease-related candidate biomarkers or therapeutic targets by finding clusters (modules) of highly correlated genes among genes across microarray samples [40]. In the present study, we successfully identified a kidney stone-related module from GSE73680 using the WGCNA method and obtained NKA. NKA participates in sodium reabsorption, calcium reabsorption and proximal tubule bicarbonate reclamation, and plays an essential role in oxidative stress.

Kidney stone has a distinct genetic predisposition. With the advancement in high-throughput sequencing technologies, SNP has become a powerful tool for mapping complex disease genes. Some nephrolithiasis-related genes, such as calcium-sensing receptor (*CASR*), vitamin D receptor (*VDR*), and osteopontin (*OPN*), have been detected with GWAS [2,41]. Although GWAS is a fundamental advance for genetic research, it requires a large sample size to maintain statistical power [2]. WES can be a good alternative approach to overcome the limitations of the GWAS study. Daga et al. detected a monogenic cause in early-onset nephrolithiasis and nephrocalcinosis by using WES in 51 families and found that WES was an efficient approach for molecular genetic diagnosis [42]. In the present study, we conducted WES on 28 patients with CaOx stones and obtained a series of candidate genes. By integrating the candidate genes with those in the salmon module from GSE73680, we discovered that *ATP1A1* may be a crucial gene for nephrolithiasis.

ATP1A1 variants have been reported in a range of diseases, such as diabetic neuropathy (rs1060366), hypertension (a functional 12T-insertion polymorphism in the *ATP1A1* promoter), aldosterone adenoma (c.311T > G and c.995T > G), and intellectual disability (c.2797G > A [p.Asp933Asn] and c.2590G > A [p.Gly864Arg]) [19–21,43]. So far, no studies are available on rs11540947. Our WES result indicated that rs11540947 in *ATP1A1* may be associated with the risk of calcium stones. We further investigated the correlation by expanding samples and determined a novel calcium stone-related SNP-rs11540947 in the 5′UTR of *ATP1A1*, which affected its promoter activity. When compared with the conventional method, we believe that the proposed method can improve the effectiveness of identifying nephrolithiasis-susceptibility genes.

Our statistical analyses revealed that rs11540947 was associated with calcium stones in men, but had no significant correlation in women, indicating that gender affects the occurrence of kidney stones. A survey of kidney stone prevalence in China indicated that the male gender was statistically significantly associated with a greater risk of kidney stones [44]. In general, men are nearly twice as likely to develop kidney stones in their lifetime than women, which may be attributed to the differences in their diet, lifestyle, sex hormones, genetics, disorders in acid-base handling, urine pH, tubular calcium reabsorption, and stone composition [45,46]. However, the gender gap in kidney stones is closing, as indicated by a recent report on the rising prevalence rise among women than in men, especially in adolescence [45].

Genetic factors explain only a part of the predisposition to stone formation, and the effect of a specific gene in the crystal formation may change with a change in the environment [2]. The injury of renal tubular epithelial cells induced by oxidative stress and inflammation is deemed an important factor for kidney stone formation [47]. Oxalate or CaOx crystals exposure promotes the excessive generation of intracellular ROS through the activation of NADPH oxidase via the renin-angiotensin-aldosterone pathway, followed by inflammation and renal tubular cell injury [48,49]. ROS production may cause the elevation of several stone-related proteins such as OPN, CD44, and MCP-1 by the activation of NF-κB and p38-MAPK/JNK, which, in turn, provide material conditions for crystal nucleation and further facilitate the crystal-cell adhesion [50]. However, the generation of ROS is a complex process involving multiple pathways. As mentioned earlier, the NKA/ROS amplification loop activated by ATP1A1/Src is an important

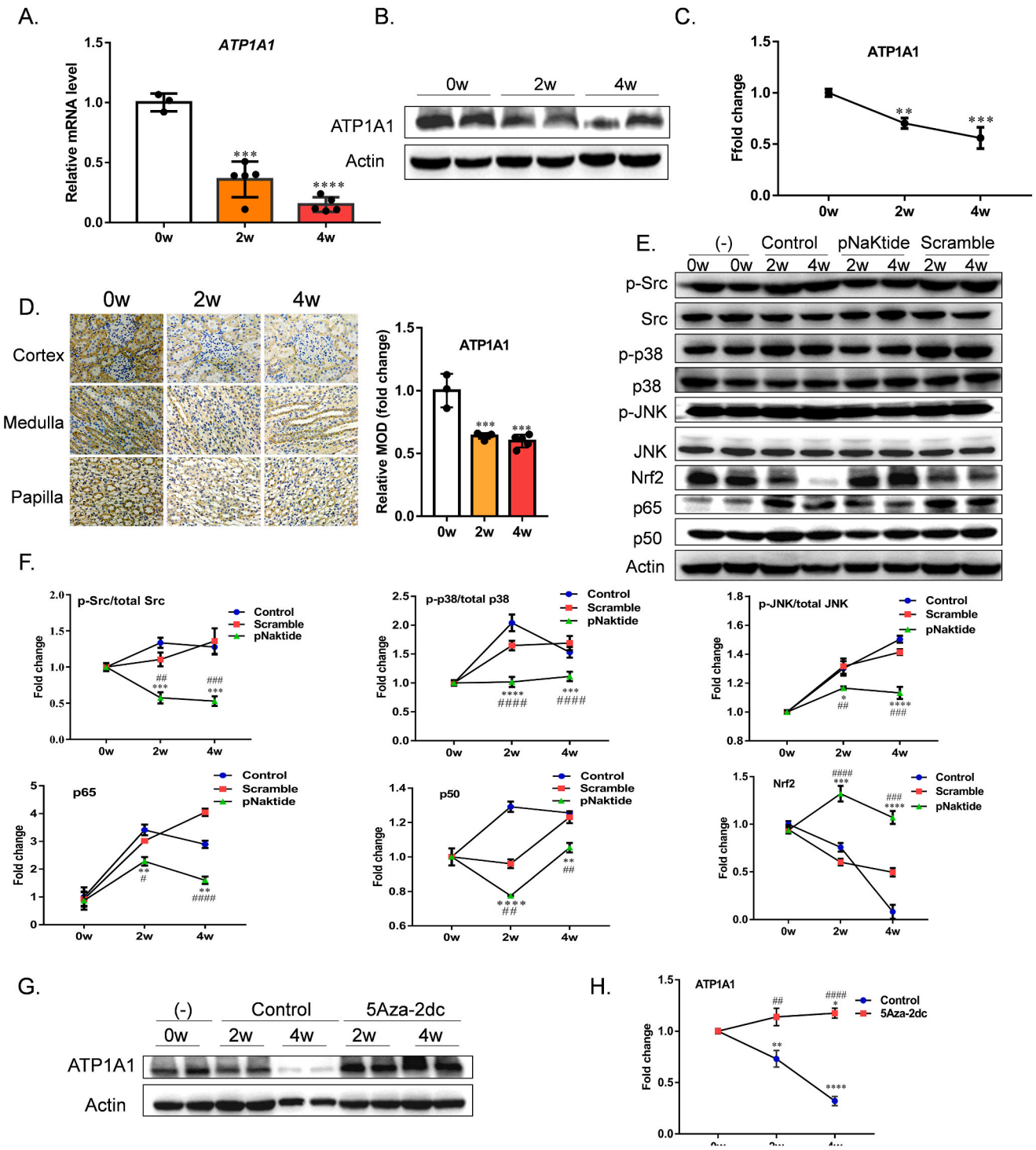

Fig. 8. The ATP1A1/Src/MAPKs/NF-κB signaling pathway was activated in the CaOx stone rat model. 0 w represents the time before inducing the CaOx stone model. The rats in the 0 w group received natural water and were used as controls (n = 3). 2 w and 4 w represent the CaOx stone rats who received water containing 20 g/L HYP and 2 g/L $CaCl_2$ for 2 and 4 weeks, respectively (n = 5 per group). (A) The mRNA level of *ATP1A1* in the rat kidneys was measured by qRT-PCR. The values were expressed as the mean ± SD (n = 3 at 0 w, n = 5 at 2 w and 4 w). ***$p < 0.001$; ****$p < 0.0001$ vs. the levels at 0 w. (B–C) The protein level of ATP1A1 in the rat kidneys was analyzed by Western blotting and was calculated as the fold change relative to the level at 0 w. The values were expressed as the mean ± SD (n = 3). **$p < 0.01$; ***$p < 0.001$ vs. the level at 0 w. (D) Immunohistochemical staining for ATP1A1 in the rat kidneys. Scale bar = 25 μM. Relative mean optical density (MOD) was calculated as the fold change relative to the value at 0 w (n = 3 at 0 w, n = 5 at 2 w and 4 w). (E–F) Western blotting analysis for the activation of Src, p38, JNK, p65, p50, and Nrf2 in the rat kidneys. The control represents the CaOx stone rats treated with 0.9% saline. Scramble and pNaKtide represent the CaOx stone rats treated with 17.5 mg/kg tat-scramble and tat-pNaKtide, respectively. The protein levels were expressed as the fold change relative to the level at 0 w. The values were expressed as the mean ± SD (n = 3). *$p < 0.05$; **$p < 0.01$; ***$p < 0.001$; ****$p < 0.0001$ vs. the control group. #$p < 0.05$; ##$p < 0.01$; ###$p < 0.001$; ####$p < 0.0001$ vs. the tat-scramble group. (G–H) The ATP1A1 protein level in rat kidneys was reversed by treatment with 1 mg/kg 5Aza-2dc. The controls represent the CaOx stone rats treated with 0.9% saline. Three independent experiments were performed. The values were expressed as the mean ± SD (n = 3). **$p < 0.01$; ****$p < 0.0001$ vs. the level at 0 w. ##$p < 0.01$; ####$p < 0.0001$ vs. the level in the control group.

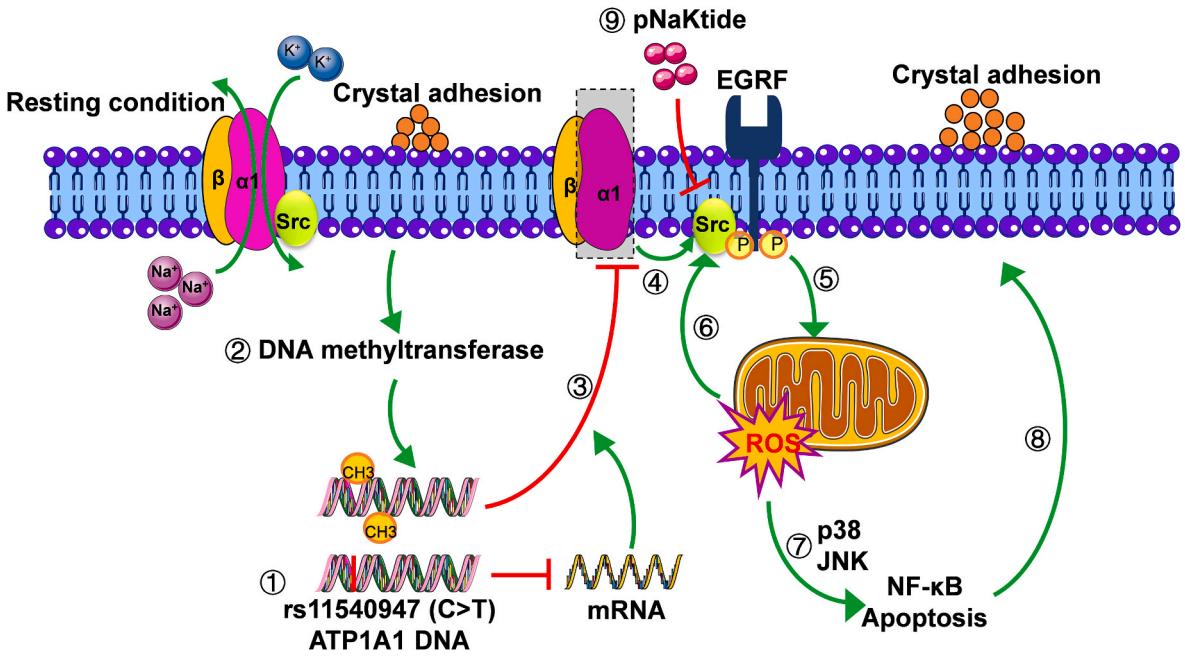

Fig. 9. A schematic diagram of the mechanism of *ATP1A1* genetic variation and ATP1A1/Src/ROS signaling pathway involved in kidney stone formation. In the resting condition, the α1 subunit encoded by *ATP1A1* gene was coupled with Src to form a receptor complex, thereby retaining the Src in an inactivated state. ① The T-allele of rs11540947 in the 5′UTR region of *ATP1A1* decreased the promoter activity. ② Crystal adhesion induced *ATP1A1* methylation by upregulating methyltransferases. ③ DNA methylation or genetic variation in *ATP1A1* decreased the expression of the α1 subunit. ④ The decreased ATP1A1 (α1, in light black box) released the Src kinase domain, which led to the phosphorylation of Src. ⑤ The activation of Src resulted in the generation of ROS. ⑥ ROS could reactivate the ATP1A1/Src signaling pathway as a ligand of the α1 subunit to form the Na/K-ATPase/ROS amplification loop. ⑦Excessive accumulation of ROS induced inflammation and apoptosis by activating the stress-related signaling pathway, including p38-MAPK and JNK. ⑧ Damaged cells further promoted crystal adhesion to the cell surface. ⑨ pNaKtide, a specific inhibitor of the ATP1A1/Src signal complex, attenuated the generation of ROS and reduced cell apoptosis and crystal-cell adhesion, thereby preventing kidney stone formation.

step in ROS production. In this study, we discovered that crystal deposition inhibited the NKA activity and the ATP1A1 expression, and activated the Src/ROS/MAPKs/NF-κB/Nrf2 signaling pathway, while the ATP1A1 overexpression effectively restrained the COM-induced ATP1A1/Src activation, oxidative stress, apoptosis and crystal-cell adhesion, thereby revealing the importance of ATP1A1 in COM-induced renal cell injury.

Our study demonstrated that both genetic variant and crystal deposition could affect the expression of *ATP1A1*, which is likely to facilitate the stone formation through two approaches. First, ATP1A1 downregulation may impair the enzymatic activity of NKA, thereby inducing an imbalance in Na^+ and K^+ concentrations, which may disturb the activity of sodium-dependent transporters in the proximal convoluted tubules, including the phosphate transporters, citrate transporter, glucose, and amino acid transporters [9], leading to the development of metabolic disorders associated with nephrolithiasis. Second, the decreased ATP1A1 expression induced renal tubular epithelial cell injury and inflammation by activating the NKA/ROS amplification loop, thereby contributing to the strengthening of crystal-cell adhesion, as confirmed by Ad-ATP1A1 infection in the present study. However, the overexpression of ATP1A1 may also prevent stone formation by regulating ion metabolism. Here, we mainly focused on the function of the ATP1A1/Src/ROS signaling pathway in stone formation as we noted that treatment with pNaKtide alone, a short peptide derived from the N domain of ATP1A1 without any ion pump activity, could alleviate COM-induced cell injury, inflammation, crystal-cell adhesion, and stone formation, thus suggesting the inhibition of ATP1A1 to stone formation mainly occurs through the action of the NKA/ROS amplification loop.

Aberrant NKA activity and expression have been implicated in diseases, and numerous factors can modulate the transcription of NKA [51]. Our research discovered that crystal deposition decreased the mRNA and protein levels of ATP1A1, suggesting the involvement of regulation at the DNA level or RNA levels in the ATP1A1 expression. DNA methylation is a vital epigenetic mechanism of gene expression that often occurs at the cytosine bases of CpG sequences in the promoter regions by DNMTs [52]. Past research has revealed that *ATP1A1* exhibits C + G rich in its promoter region [35], implying that DNA methylation possibly participates in regulating the ATP1A1 expression. We also found that COM exposure significantly increased the mRNA and protein levels of DNMT1, DNMT3a, and DNMT3b. These enzymes were finely regulated, and the deregulation of their expression possibly led to abnormal methylation [53]. Treatment with a specific inhibitor of DNA methyltransferase both *in vitro* and *in vivo* inhibited the downregulation of ATP1A1 induced by crystal deposition, thus validating that altered-DNA methylation was the primary mechanism of CaOx-induced ATP1A1 decrease in our study, although different regulation manners for the ATP1A1 expression have been reported, such as endocytosis and oxidative degradation [54,55]. In addition, DNA cytosine methylation impacts the mutation rates through spontaneous oxidative deamination of 5-methylcytosine to thymine, which may explain the accumulation of C > T human somatic mutations [56]. Taken together, to the best of our knowledge, the alteration of DNA methylation noted in the present study is a novel regulative mechanism for CaOx-induced gene expression.

There are still some limitations to our research. First, the kidney tissues, urine samples, and some key clinical data of the patients were not collected. Hence, the genetic variation and expression of ATP1A1 could not be more precisely correlated with the patient's phenotype. Second, although we noted that crystal deposition could regulate the expression of ATP1A1 through the alteration of DNA methylation, there was no direct evidence demonstrating that crystal deposition induced hypermethylation of *ATP1A1* as the previous and the present studies have not reported a suitable probe due to a particular gene sequence of *ATP1A1* [57].

In conclusion, the present study demonstrated, for the first time, that

ATP1A1, as a gene influenced by both genetic and environmental factors, plays a crucial role in the formation of CaOx stones through an integrated omics approach and cell biology technologies. Our findings may provide a potentially effective strategy for targeting *ATP1A1* in the treatment of kidney stones, at least for CaOx stones.

Funding

The study was supported by a grant of National Natural Science Foundation of China (No. 82070722) and Liaoning Provincial Innovation Capacity Promotion Joint Fund (2022-NLTS-14-07).

Author contributions

Xiuli Lu and Bing Gao conceived of the idea of this study. Yang Li, Haozhen Wang, and Zhihao Yu performed the experiments and analyzed the data. Yang Li and Xiuli Lu wrote the manuscript, Xiuli Lu and Bing Gao revised the manuscript. All authors have reviewed and approved the paper.

Declaration of competing interest

All the authors declare that they have no conflict of interest.

Data availability

Data will be made available on request.

Acknowledgments

We thank Takahiro Yasui et al. from the Department of Nephro-urology, Nagoya City University Graduate School of Medical Sciences for providing the gene expression profiles (GSE73680).

Appendix A. Supplementary data

Supplementary data to this article can be found online at https://doi.org/10.1016/j.redox.2023.102648.

References

[1] E. Worcester, F. Coe, Nephrolithiasis, Primary care. 35 (2008) 369–391, https://doi.org/10.1016/j.pop.2008.01.005, vii.
[2] T. Yasui, A. Okada, S. Hamamoto, et al., Pathophysiology-based treatment of urolithiasis, Int. J. Urol. 24 (2017) 32–38, https://doi.org/10.1111/iju.13187.
[3] V. Thongboonkerd, Proteomics of crystal-cell interactions: a model for kidney stone research, Cells 8 (2019), https://doi.org/10.3390/cells8091076.
[4] J.H. Wiessner, A.T. Hasegawa, L.Y. Hung, et al., Mechanisms of calcium oxalate crystal attachment to injured renal collecting duct cells, Kidney Int. 59 (2001) 637–644, https://doi.org/10.1046/j.1523-1755.2001.059002637.x.
[5] K. Niimi, T. Yasui, M. Hirose, et al., Mitochondrial permeability transition pore opening induces the initial process of renal calcium crystallization, Free Radic. Biol. Med. 52 (2012) 1207–1217, https://doi.org/10.1016/j.freeradbiomed.2012.01.005.
[6] S.R. Khan, R.L. Hackett, Retention of calcium oxalate crystals in renal tubules, Scanning Microsc. 5 (1991) 707–711, discussion 11-2.
[7] M. Hirose, K. Tozawa, A. Okada, et al., Glyoxylate induces renal tubular cell injury and microstructural changes in experimental mouse, Urol. Res. 36 (2008) 139–147, https://doi.org/10.1007/s00240-008-0143-7.
[8] S. Pirkmajer, A. Chibalin, Hormonal regulation of Na-K-ATPase from the evolutionary perspective, Curr. Top. Membr. 83 (2019) 315–351, https://doi.org/10.1016/bs.ctm.2019.01.009.
[9] V. Walker, Phosphaturia in kidney stone formers: still an enigma, Adv. Clin. Chem. 90 (2019) 133–196, https://doi.org/10.1016/bs.acc.2019.01.004.
[10] A. Aperia, Homer Smith Award: to serve and protect: classic and novel roles for Na+, K+ -adenosine triphosphatase, J. Am. Soc. Nephrol. : JASN (J. Am. Soc. Nephrol.) 23 (2011) 1283–1290, https://doi.org/10.1681/asn.2012010102, 2012.
[11] J. Tian, T. Cai, Z. Yuan, et al., Binding of Src to Na+/K+-ATPase forms a functional signaling complex, Mol. Biol. Cell 17 (2006) 317–326, https://doi.org/10.1091/mbc.e05-08-0735.
[12] Y. Wang, Q. Ye, C. Liu, et al., Involvement of Na/K-ATPase in hydrogen peroxide-induced activation of the Src/ERK pathway in LLC-PK1 cells, Free Radic. Biol. Med. 71 (2014) 415–426, https://doi.org/10.1016/j.freeradbiomed.2014.03.036.
[13] Z. Li, T. Cai, J. Tian, et al., NaKtide, a Na/K-ATPase-derived peptide Src inhibitor, antagonizes ouabain-activated signal transduction in cultured cells, J. Biol. Chem. 284 (2009) 21066–21076, https://doi.org/10.1074/jbc.M109.013821.
[14] Y. Yan, J.I. Shapiro, The physiological and clinical importance of sodium potassium ATPase in cardiovascular diseases, Curr. Opin. Pharmacol. 27 (2016) 43–49, https://doi.org/10.1016/j.coph.2016.01.009.
[15] K. Srikanthan, J.I. Shapiro, K. Sodhi, The role of Na/K-ATPase signaling in oxidative stress related to obesity and cardiovascular disease, Molecules 21 (2016), https://doi.org/10.3390/molecules21091172.
[16] Y. An, H. Zhang, C. Wang, et al., Activation of ROS/MAPKs/NF-κB/NLRP3 and inhibition of efferocytosis in osteoclast-mediated diabetic osteoporosis, Faseb. J. 33 (2019) 12515–12527, https://doi.org/10.1096/fj.201802805RR.
[17] J. Xiao, X. Zhang, C. Fu, et al., Impaired Na(+)-K(+)-ATPase signaling in renal proximal tubule contributes to hyperuricemia-induced renal tubular injury, Exp. Mol. Med. 50 (2018) e452, https://doi.org/10.1038/emm.2017.287.
[18] D.E. Bartlett, R.B. Miller, S. Thiesfeldt, et al., Uremic toxins activates Na/K-ATPase oxidant amplification loop causing phenotypic changes in adipocytes in in vitro models, Int. J. Mol. Sci. 19 (2018), https://doi.org/10.3390/ijms19092685.
[19] M.A. Abosheasha, F. Zahran, S.S. Bessa, et al., Association between a novel G94A single nucleotide polymorphism in ATP1A1 gene and type 2 diabetes mellitus among Egyptian patients, J. Res. Med. Sci. : Off. J. Isfahan Univ. Med. Sci. 24 (2019) 62, https://doi.org/10.4103/jrms.JRMS_975_18.
[20] F. Beuschlein, S. Boulkroun, A. Osswald, et al., Somatic mutations in ATP1A1 and ATP2B3 lead to aldosterone-producing adenomas and secondary hypertension, Nat. Genet. 45 (2013) 440–444, https://doi.org/10.1038/ng.2550, 4e1-2.
[21] Z. Lin, J. Li, T. Ji, et al., ATP1A1 de novo mutation-related disorders: clinical and genetic features, Frontiers. Pediatric. 9 (2021), 657256, https://doi.org/10.3389/fped.2021.657256.
[22] R. Palsson, O.S. Indridason, V.O. Edvardsson, et al., Genetics of common complex kidney stone disease: insights from genome-wide association studies, Urolithiasis 47 (2019) 11–21, https://doi.org/10.1007/s00240-018-1094-2.
[23] K. Taguchi, S. Hamamoto, A. Okada, et al., Genome-wide gene expression profiling of randall's plaques in calcium oxalate stone formers, J. Am. Soc. Nephrol. : JASN (J. Am. Soc. Nephrol.) 28 (2017) 333–347, https://doi.org/10.1681/asn.2015111271.
[24] C.A. Wright, S. Howles, D.C. Trudgian, et al., Label-free quantitative proteomics reveals differentially regulated proteins influencing urolithiasis, Mol. Cell. Proteomics 10 (2011), M110.005686, https://doi.org/10.1074/mcp.M110.005686.
[25] B. Yang, X. Lu, Y. Li, et al., A proteomic network approach across the kidney stone disease reveals endoplasmic reticulum stress and crystal-cell interaction in the kidney, Oxid. Med. Cell. Longev. (2019), 9307256, https://doi.org/10.1155/2019/9307256, 2019.
[26] K. Karczewski, M. Snyder, Integrative omics for health and disease, Nat. Rev. Genet. 19 (2018) 299–310, https://doi.org/10.1038/nrg.2018.4.
[27] H. Li, A. Yin, Z. Cheng, et al., Attenuation of Na/K-ATPase/Src/ROS amplification signal pathway with pNaktide ameliorates myocardial ischemia-reperfusion injury, Int. J. Biol. Macromol. 118 (2018) 1142–1148, https://doi.org/10.1016/j.ijbiomac.2018.07.001.
[28] Y. Li, X. Wang, B. Yang, et al., 3β-Hydroxysteroid-Δ24 reductase (DHCR24) protects pancreatic β cells from endoplasmic reticulum stress-induced apoptosis by scavenging excessive intracellular reactive oxygen species, J. Diabetes Res. (2020), 3426902, https://doi.org/10.1155/2020/3426902, 2020.
[29] M. Le Dudal, L. Huguet, J. Perez, et al., Stiripentol protects against calcium oxalate nephrolithiasis and ethylene glycol poisoning, J. Clin. Investig. 129 (2019) 2571–2577, https://doi.org/10.1172/jci99822.
[30] J. Liu, J. Tian, M. Chaudhry, et al., Attenuation of Na/K-ATPase mediated oxidant amplification with pNaKtide ameliorates experimental uremic cardiomyopathy, Sci. Rep. 6 (2016), 34592, https://doi.org/10.1038/srep34592.
[31] J. Chen, X. Zhang, H. Zhang, et al., Indoxyl sulfate enhance the hypermethylation of klotho and promote the process of vascular calcification in chronic kidney disease, Int. J. Biol. Sci. 12 (2016) 1236–1246, https://doi.org/10.7150/ijbs.15195.
[32] R. Manek, T. Nelson, E. Tseng, et al., 5'UTR-mediated regulation of Ataxin-1 expression, Neurobiol. Dis. 134 (2020), 104564, https://doi.org/10.1016/j.nbd.2019.104564.
[33] E. Dumas, C. Staedel, M. Colombat, et al., A promoter activity is present in the DNA sequence corresponding to the hepatitis C virus 5' UTR, Nucleic Acids Res. 31 (2003) 1275–1281, https://doi.org/10.1093/nar/gkg199.
[34] Y. Miyamoto, A. Mabuchi, D. Shi, et al., A functional polymorphism in the 5' UTR of GDF5 is associated with susceptibility to osteoarthritis, Nat. Genet. 39 (2007) 529–533, https://doi.org/10.1038/2005.
[35] M.M. Shull, D.G. Pugh, J.B. Lingrel, The human Na, K-ATPase alpha 1 gene: characterization of the 5'-flanking region and identification of a restriction fragment length polymorphism, Genomics 6 (1990) 451–460, https://doi.org/10.1016/0888-7543(90)90475-a.
[36] T.W. Kensler, N. Wakabayashi, S. Biswal, Cell survival responses to environmental stresses via the Keap1-Nrf2-ARE pathway, Annu. Rev. Pharmacol. Toxicol. 47 (2007) 89–116, https://doi.org/10.1146/annurev.pharmtox.46.120604.141046.
[37] S.R. Khan, K.J. Byer, S. Thamilselvan, et al., Crystal-cell interaction and apoptosis in oxalate-associated injury of renal epithelial cells, J. Am. Soc. Nephrol. : JASN (J. Am. Soc. Nephrol.) 10 (14) (1999) S457–S463.
[38] L.C. Cao, J. Jonassen, T.W. Honeyman, et al., Oxalate-induced redistribution of phosphatidylserine in renal epithelial cells: implications for kidney stone disease, Am. J. Nephrol. 21 (2001) 69–77, https://doi.org/10.1159/000046224.

[39] R.J. Klose, A.P. Bird, Genomic DNA methylation: the mark and its mediators, Trends Biochem. Sci. 31 (2006) 89–97, https://doi.org/10.1016/j.tibs.2005.12.008.
[40] P. Langfelder, S. Horvath, WGCNA: an R package for weighted correlation network analysis, BMC Bioinf. 9 (2008) 559, https://doi.org/10.1186/1471-2105-9-559.
[41] J. Sayer, Progress in understanding the genetics of calcium-containing nephrolithiasis, J. Am. Soc. Nephrol. : JASN (J. Am. Soc. Nephrol.) 28 (2017) 748–759, https://doi.org/10.1681/asn.2016050576.
[42] A. Daga, A.J. Majmundar, D.A. Braun, et al., Whole exome sequencing frequently detects a monogenic cause in early onset nephrolithiasis and nephrocalcinosis, Kidney Int. 93 (2018) 204–213, https://doi.org/10.1016/j.kint.2017.06.025.
[43] V. Herrera, K. Pasion, A. Moran, et al., A functional 12T-insertion polymorphism in the ATP1A1 promoter confers decreased susceptibility to hypertension in a male Sardinian population, PLoS One 10 (2015), e0116724, https://doi.org/10.1371/journal.pone.0116724.
[44] G. Zeng, Z. Mai, S. Xia, et al., Prevalence of kidney stones in China: an ultrasonography based cross-sectional study, BJU Int. 120 (2017) 109–116, https://doi.org/10.1111/bju.13828.
[45] K. Gillams, P. Juliebø-Jones, S. Juliebø, et al., Gender differences in kidney stone disease (KSD): findings from a systematic Review, Curr. Urol. Rep. 22 (2021) 50, https://doi.org/10.1007/s11934-021-01066-6.
[46] P.M. Ferraro, T.D.S. Cunha, G.C. Curhan, Sex differences and the risk of kidney stones, Semin. Nephrol. 42 (2022) 230–235, https://doi.org/10.1016/j.semnephrol.2022.04.012.
[47] Y. Wu, Y. Xun, J. Zhang, et al., Resveratrol attenuates oxalate-induced renal oxidative injury and calcium oxalate crystal deposition by regulating TFEB-induced autophagy pathway, Front. Cell Dev. Biol. 9 (2021), 638759, https://doi.org/10.3389/fcell.2021.638759.
[48] J. Zhang, Q. Wang, C. Xu, et al., MitoTEMPO prevents oxalate induced injury in NRK-52e cells via inhibiting mitochondrial dysfunction and modulating oxidative stress, Oxid. Med. Cell. Longev. (2017), 7528090, https://doi.org/10.1155/2017/7528090, 2017.
[49] H. Tsuji, W. Wang, J. Sunil, et al., Involvement of renin-angiotensin-aldosterone system in calcium oxalate crystal induced activation of NADPH oxidase and renal cell injury, World J. Urol. 34 (2016) 89–95, https://doi.org/10.1007/s00345-015-1563-y.
[50] S.R. Khan, Reactive oxygen species as the molecular modulators of calcium oxalate kidney stone formation: evidence from clinical and experimental investigations, J. Urol. 189 (2013) 803–811, https://doi.org/10.1016/j.juro.2012.05.078.
[51] Z. Li, S. Langhans, Transcriptional regulators of Na,K-ATPase subunits, Front. Cell Dev. Biol. 3 (2015) 66, https://doi.org/10.3389/fcell.2015.00066.
[52] H. Cedar, Y. Bergman, Linking DNA methylation and histone modification: patterns and paradigms, Nat. Rev. Genet. 10 (2009) 295–304, https://doi.org/10.1038/nrg2540.
[53] J. Loaeza-Loaeza, A.S. Beltran, D. Hernández-Sotelo, DNMTs and impact of CpG content, transcription factors, consensus motifs, lncRNAs, and histone marks on DNA methylation, Genes 11 (2020), https://doi.org/10.3390/genes11111336.
[54] J. Liu, Y. Nie, M. Chaudhry, et al., The redox-sensitive Na/K-ATPase signaling in uremic cardiomyopathy, Int. J. Mol. Sci. 21 (2020), https://doi.org/10.3390/ijms21041256.
[55] J. Liu, M. Liang, L. Liu, et al., Ouabain-induced endocytosis of the plasmalemmal Na/K-ATPase in LLC-PK1 cells requires caveolin-1, Kidney Int. 67 (2005) 1844–1854, https://doi.org/10.1111/j.1523-1755.2005.00283.x.
[56] J. Yang, J.R. Horton, K.C. Akdemir, et al., Preferential CEBP binding to T:G mismatches and increased C-to-T human somatic mutations, Nucleic Acids Res. 49 (2021) 5084–5094, https://doi.org/10.1093/nar/gkab276.
[57] I.A. Deckers, M. van Engeland, P.A. van den Brandt, et al., Promoter CpG island methylation in ion transport mechanisms and associated dietary intakes jointly influence the risk of clear-cell renal cell cancer, Int. J. Epidemiol. 46 (2017) 622–631, https://doi.org/10.1093/ije/dyw266.